Periodic Preamble-Based Frequency Recovery in OFDM Receivers Plagued by I/Q Imbalance

Antonio A. D'Amico, Michele Morelli, *Senior Member, IEEE*, and Marco Moretti , *Member, IEEE*

***Abstract*— The direct conversion receiver (DCR) architecture has received much attention in the last few years as an effective means to obtain user terminals with reduced cost, size, and power consumption. A major drawback of a DCR device is the possible insertion of in-phase/quadrature imbalances in the demodulated signal, which can seriously degrade the performance of conventional synchronization algorithms. In this paper, we investigate the problem of carrier frequency offset (CFO) recovery in an orthogonal frequency-division multiplexing receiver equipped with a DCR front-end. Our approach is based on maximum likelihood (ML) arguments and aims at jointly estimating the CFO, the useful signal component, and its mirror image. In doing so, we exploit knowledge of the pilot symbols transmitted within a conventional repeated training preamble appended in front of each data packet. Since the exact ML solution turns out to be too complex for practical purposes, we propose two alternative schemes which can provide nearly optimal performance with substantial computational saving. One of them provides the CFO in closed-form, thereby avoiding any grid-search procedure. The accuracy of the proposed methods is assessed in a scenario compliant with the 802.11a WLAN standard. Compared to existing solutions, the novel schemes achieve improved performance at the price of a tolerable increase of the processing load.**

***Index Terms*— Carrier frequency estimation, OFDM, direct-conversion receiver, I/Q imbalance.**

I. Introduction

ORTHOGONAL frequency-division multiplexing (OFDM) is a popular multicarrier technology which offers remarkable resilience against multipath distortions, increased spectral efficiency, and the possibility of performing adaptive modulation and coding. Due to such potential advantages, it has been adopted in several wideband commercial systems, including the IEEE 802.11a wireless local area network (WLAN) [1], the IEEE 802.16 wireless metropolitan area network (WMAN) [2], and the 3GPP long-term evolution (LTE) [3]. Recent studies indicate that the use of a direct-conversion receiver (DCR) in combination with the OFDM technology can provide an effective means for the implementation of user terminals with reduced size and power consumption [4]. These advantages are achieved through elimination of expensive intermediate frequency (IF) filters and other off-chip components employed in the classical superheterodyne architecture. The price is a higher degree of radio-frequency (RF) imperfections arising from the use of analog in-phase/quadrature (I/Q) low-pass filters (LPF) with mismatched frequency responses, and from local oscillator (LO) signals with amplitude and phase imbalances. In general, LO-induced distortions are nearly flat in the frequency domain, while filter mismatches can vary substantially over the signal bandwidth, especially in a wideband communication system [5]. If not properly compensated, the I/Q imbalance introduces image interference from mirrored subcarriers, with ensuing limitations of the system performance. In addition to I/Q imperfections, an OFDM receiver is also vulnerable to the carrier frequency offset (CFO) between the incoming waveform and the LO signals, which generates interchannel interference in the demodulated signal.

In recent years, an intense research activity has been conducted to investigate the problem of CFO recovery in OFDM systems plagued by frequency-selective I/Q imperfections. Many available solutions operate in the time-domain and exploit a suitably designed training preamble (TP) appended in front of the data packet. For example, the authors of [6] and [7] recover the cosine of the CFO by using a TP composed of three repeated segments. However, due to the even property of the cosine function, the estimated frequency is affected by a inherent sign ambiguity, which severely limits the accuracy in case of small CFO values. Some feasible solutions to fix the sign ambiguity problem are presented in [8]–[10], where the original TP of [6] is properly extended so as to retrieve both the cosine and the sine of the CFO. Unambiguous frequency estimates are also obtained in [11] and [12] by exploiting a TP composed of several repeated parts, which are rotated by a specific phase pattern before being transmitted. Unfortunately, the resulting schemes are not computationally efficient as they require a grid-search over the uncertainty frequency interval. The same problem occurs in [13] and [14], where no closed-form solution is provided to get the CFO estimate. A low-complexity scheme is presented in [15] to jointly compensate for the CFO and I/Q imbalances without resorting to any grid-search procedure.

The main drawback of the aforementioned methods is that they rely on specific TPs that cannot be found in any OFDM communication standard. Alternative schemes employing the IEEE 802.11a conventional repeated TP can be found

Manuscript received March 2, 2017; revised July 5, 2017 and September 26, 2017; accepted September 29, 2017. The associate editor coordinating the review of this paper and approving it for publication was J. M. Romero-Jerez. *(Corresponding author: Marco Moretti.)*

The authors are with the Dipartimento di Ingegneria dell'Informazione, University of Pisa, 56126 Pisa, Italy (e-mail: marco.moretti@iet.unipi.it).

Color versions of one or more of the figures in this paper are available online at http://ieeexplore.ieee.org.

in [16]–[20]. In particular, novel sine- and cosine-based estimators are derived in [16] by means of a suitable matrix formulation of the received signal samples, while a linear least squares estimation of the unsigned CFO is formulated in [18] using a general relationship among three adjacent TP segments. In [19] and [20], the useful signal component and its mirror image are interpreted as two independent sinusoidal signals, which are separated by resorting to either the ESPRIT (estimation of signal parameters via rotational invariance technique [21]) or the SAGE (space-alternating generalized expectation-maximization [22]) algorithms, respectively. In [23] the authors show that, at low and medium signal-to-noise ratio (SNR) values, the classical maximum likelihood (CML) frequency estimator, derived in [24] for a perfectly balanced receiver, performs satisfactorily even in the presence of some I/Q imbalance. Furthermore, in many situations CML exhibits improved accuracy with respect to the joint maximum likelihood (JML) estimator of the CFO, the channel distorted TP and its mirror image, which was originally presented in [11]. The reason is that JML, when applied to a repetitive TP, is subject to the sign ambiguity problem and provides poor results in the presence of small CFO values. A novel frequency estimator is also derived in [23] by exploiting some side-information about the signal-to-image ratio. This scheme, which is named constrained JML (CJML), can achieve improved accuracy with respect to CML and JML at the price of a substantial increase of the computational burden. Finally, a low-complexity scheme for the joint estimation of the CFO, channel impulse response (CIR) and I/Q imbalance is presented in [25] using the long training sequence embedded in the 802.11a preamble.

In this work, we consider an OFDM direct-conversion receiver affected by frequency-selective I/Q imbalances and further investigate the CFO recovery task using a repeated TP. In order to remove the sign ambiguity problem that affects the JML, the joint estimation of the CFO and channel impulse responses for the signal component and its mirror image is accomplished by suitably exploiting knowledge of the pilot symbols embedded in the received TP. Unfortunately, the exact ML solution cannot be implemented in practice due to its prohibitive processing requirements. Therefore, we look for simpler solutions that can be executed with affordable complexity. One of them is an approximation of the true ML estimator, which is obtained by neglecting the phase rotation induced by the residual CFO within each TP segment. The resulting scheme allows a substantial reduction of the system complexity without incurring any significant penalty in estimation accuracy with respect to the ML estimator. We also derive an alternative method based on the best linear unbiased estimation (BLUE) principle, which further reduces the processing requirements by computing the CFO estimate in closed-form. Numerical simulations indicate that the proposed schemes perform satisfactorily even in the presence of severe I/Q imbalances and outperform other existing methods. Their performance is close to the Cramer-Rao bound (CRB) provided that the order of the *overall* propagation channel (comprising the transmit and receive filters) does not exceed half the number of the pilot symbols of the TP.

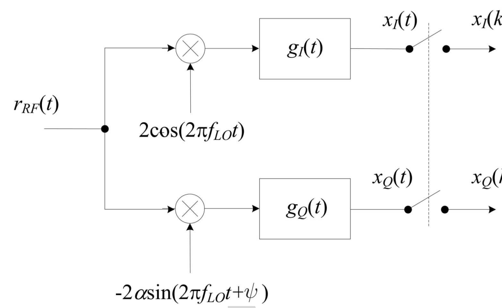

Fig. 1. Basic DCR architecture.

When such a condition is not met, the estimation accuracy decreases, especially at high SNR values.

The rest of the paper is organized as follows. Next section describes the DCR architecture and introduces the mathematical model of the received TP. In Sect. III we discuss the joint ML estimation of the CFO and channel impulse responses for the useful signal and its mirror image. Some practical adjustments are also suggested to reduce the processing load of the ML scheme. In Sect. IV we adopt the BLUE concept to get the CFO estimate in closed-form, while in Sect. V we present the CRB analysis for the considered estimation problem. Simulation results are presented in Sect. VI and, finally, some conclusions are offered in Sect. VII.

Notation: Matrices and vectors are denoted by boldface letters, with $\mathbf{I}_N$ and $\mathbf{1}_N$ being the identity matrix of order N and the N-dimensional vector with unit entries, respectively. $\mathbf{A} = \text{diag}\{a(n)\,;\ n = 1, 2, \ldots, N\}$ denotes an $N \times N$ diagonal matrix with entries $a(n)$ along its main diagonal, $[\mathbf{C}]_{k,\ell}$ is the (k, ℓ)th entry of $\mathbf{C}$ and $\mathbf{B}^{-1}$ is the inverse of a matrix $\mathbf{B}$. The notation $\|\cdot\|$ represents the Euclidean norm of the enclosed vector while $\Re\text{e}\{x\}$, $\Im\text{m}\{x\}$, $|x|$ and $\arg\{x\}$ stand for the real and imaginary parts, the modulus, and the principal argument of a complex number x. The symbol $\otimes$ is adopted for either the convolution between continuous-time signals or the Kronecker product between matrices and/or vectors. We use $\text{E}\{\cdot\}$, $(\cdot)^*$, $(\cdot)^T$ and $(\cdot)^H$ for expectation, complex conjugation, transposition and Hermitian transposition, respectively. Finally, $\tilde{\lambda}$ denotes a trial value of the unknown parameter λ.

II. System Model in the Presence of CFO and I/Q Imbalance

A. DCR Architecture

Fig. 1 illustrates the basic structure of a DCR front-end. Here, the received RF waveform $r_{RF}(t)$ is down-converted to baseband using LO signals characterized by an amplitude mismatch α and a phase error ψ. The demodulated signals are then fed to I/Q low-pass filters with different impulse responses $g_I(t)$ and $g_Q(t)$. While LO imperfections give rise to frequency-independent I/Q imbalances, filter mismatches vary over the signal bandwidth, thereby resulting into a frequency-selective imbalance [11]. We call $r(t)$ the complex envelope of $r_{RF}(t)$ with respect to the carrier frequency f_0, and let $\Delta f = f_0 - f_{LO}$ be the offset between the carrier and LO frequencies. Hence, we can write the received waveform as $r_{RF}(t) = \Re\text{e}\{r(t)e^{j2\pi(f_{LO}+\Delta f)t}\}$, with

$$r(t) = s(t) \otimes v(t) + n(t). \tag{1}$$

In the above equation, $s(t)$ and $v(t)$ are the baseband representations of the transmitted signal and propagation channel, respectively, while $n(t)$ is circularly symmetric AWGN with two-sided power spectral density $2N_0$. As shown in Fig. 1, we denote by $x(t) = x_I(t) + jx_Q(t)$ the complex down-converted signal at the output of the mismatched I/Q filters. Then, after standard manipulations we get

$$x(t) = e^{j2\pi\Delta f t}[s(t) \otimes h(t)] + e^{-j2\pi\Delta f t}[s^*(t) \otimes q(t)] + w(t) \tag{2}$$

where the first term is the direct signal component, the second term represents self-image interference, and $w(t)$ accounts for the noise contribution. The equivalent CIRs $h(t)$ and $q(t)$ appearing in (2) are expressed by [11]

$$\begin{aligned} h(t) &= v(t) \otimes p_+(t)e^{-j2\pi\Delta f t} \\ q(t) &= v^*(t) \otimes p_-(t)e^{j2\pi\Delta f t} \end{aligned} \tag{3}$$

with

$$\begin{aligned} p_+(t) &= \frac{1}{2}[g_I(t) + \alpha g_Q(t)e^{-j\psi}] \\ p_-(t) &= \frac{1}{2}[g_I(t) - \alpha g_Q(t)e^{j\psi}] \end{aligned} \tag{4}$$

while the noise term $w(t) = w_I(t) + jw_Q(t)$ takes the form

$$w(t) = n(t)e^{j2\pi\Delta f t} \otimes p_+(t) + n^*(t)e^{-j2\pi\Delta f t} \otimes p_-(t). \tag{5}$$

Substituting (4) into (5), it is found that $w_I(t)$ and $w_Q(t)$ are zero-mean Gaussian processes with auto- and cross-correlation functions

$$\begin{aligned} \mathrm{E}\{w_I(t)w_I(t+\tau)\} &= N_0[g_I(\tau) \otimes g_I(-\tau)] \\ \mathrm{E}\{w_Q(t)w_Q(t+\tau)\} &= \alpha^2 N_0[g_Q(\tau) \otimes g_Q(-\tau)] \\ \mathrm{E}\{w_I(t)w_Q(t+\tau)\} &= -\alpha N_0 \sin\psi[g_I(\tau) \otimes g_Q(-\tau)]. \end{aligned} \tag{6}$$

Since the real and imaginary components of $w(t)$ are generally cross-correlated with different auto-correlation functions, we conclude that, in general, the noise process at the ouptut of a DCR front-end is not circularly symmetric.

B. Mathematical Model of the Received TP

We consider an OFDM burst-mode communication system, where each burst is preceded by a TP to assist the synchronization and channel estimation functions. In contrast to many related works, where the TP is suitably designed to cope with I/Q imbalances [6]–[15], in this study we assume a conventional periodic preamble composed by $M_T \geq 2$ repeated segments. Each segment contains P time-domain samples, which are obtained as the inverse discrete Fourier transform (IDFT) of P pilot symbols $\{c(n); n = 0, 1, \ldots, P-1\}$. Such a preamble is general enough to include both the short training sequence ($M_T = 10$, $P = 16$) and the long training sequence ($M_T = 2$, $P = 64$) of the 802.11a WLAN standard [1]. In the former case, a number $M_G \geq 1$ of segments serve as a cyclic prefix (CP) to avoid interblock interference, while the remaining $M = M_T - M_G$ segments are exploited for synchronization purposes. In the latter case we have $M_G = 0$ since the long training sequence is preceded by its own CP.

For simplicity, we consider a discrete-time baseband signal model with signaling interval T_s. The TP samples are thus given by

$$s[l] = \frac{1}{\sqrt{P}} \sum_{n=0}^{P-1} c(n)e^{j2\pi nl/P} \quad -N_G \leq l \leq MP-1 \tag{7}$$

where N_G is the CP duration normalized by T_s. After propagating through the multipath channel, the received signal $x[l] = x(lT_s)$ is plagued by CFO and frequency-selective I/Q imbalances. Bearing in mind (2) and assuming that $h(t)$ and $q(t)$ have support $[0, LT_s)$ with $L \leq N_G$, we have

$$\begin{aligned} x[l] = {} & \frac{e^{jl\phi}}{\sqrt{P}} \sum_{k=0}^{L-1} h[k] \sum_{n=0}^{P-1} c(n)e^{j2\pi n(l-k)/P} \\ & + \frac{e^{-jl\phi}}{\sqrt{P}} \sum_{k=0}^{L-1} q[k] \sum_{n=0}^{P-1} c^*(n)e^{-j2\pi n(l-k)/P} + w[l] \end{aligned} \tag{8}$$

for $0 \leq l \leq MP-1$. In the above equation, $h[k]$ and $q[k]$ is the shorthand notation for $h(kT_s)$ and $q(kT_s)$, respectively, $w[l]$ is the noise sample and we have defined

$$\phi = 2\pi\Delta f T_s. \tag{9}$$

To proceed further, we arrange the quantities $x[l]$ into an $MP-$ dimensional vector $\mathbf{x} = (x[0], x[1], \ldots, x[MP-1])^T$ and let $\mathbf{C} = \mathrm{diag}\{c(n),\ n = 0, 1, \ldots, P-1\}$. Then, we can put (8) in matrix notation as

$$\mathbf{x} = \mathbf{\Gamma}(\phi)\mathbf{G}_1\mathbf{C}\mathbf{G}_2\mathbf{h} + \mathbf{\Gamma}(-\phi)\mathbf{G}_1^*\mathbf{C}^*\mathbf{G}_2^*\mathbf{q} + \mathbf{w} \tag{10}$$

where $\mathbf{h} = (h[0],\ h[1], \ldots, h[L-1])^T$ and $\mathbf{q} = (q[0], q[1], \ldots, q[L-1])^T$ are the $L-$dimensional CIR vectors, $\mathbf{w} = (w[0],\ w[1], \ldots, w[MP-1])^T$ represents the noise contribution and $\mathbf{\Gamma}(\phi) = \mathrm{diag}\{e^{jl\phi},\ l = 0, 1, \ldots, MP-1\}$. Finally, $\mathbf{G}_2$ is a $(P \times L)-$dimensional matrix with entries

$$[\mathbf{G}_2]_{n,k} = e^{-j2\pi(n-1)(k-1)/P} \quad n = 1, 2, \ldots, P \;\; k = 1, 2, \ldots, L \tag{11}$$

while $\mathbf{G}_1$ has dimension $MP \times P$ and can be expressed as

$$\mathbf{G}_1 = \mathbf{1}_M \otimes \mathbf{F}_P \tag{12}$$

where $\mathbf{F}_P$ is the unitary $P-$point IDFT matrix with entries

$$[\mathbf{F}_P]_{n,k} = \frac{1}{\sqrt{P}} e^{j2\pi(n-1)(k-1)/P} \quad n, k = 1, 2, \ldots, P. \tag{13}$$

III. Joint ML Estimation of the CFO and CIR Vectors

A. Estimator Design

Inspection of (3) and (4) indicates that the equivalent CIRs $h(t)$ and $q(t)$ are mathematically related to the LO imbalance parameters α and ψ, the CFO Δf and the propagation channel $v(t)$. All these quantities can in principle be recovered from the observation vector $\mathbf{x}$ by resorting to some optimality criterion. Albeit effective, this approach would result into a prohibitively complex estimation process, where an exhaustive grid-search has to be employed to localize the optimum point of a multidimensional cost function. For this reason, we follow a more pragmatic strategy, which ignores the dependence of $\mathbf{u} = [\mathbf{h}^T \ \ \mathbf{q}^T]^T$ on the other unknown parameters and looks for the joint ML estimates of ($\mathbf{u}$, ϕ). Despite the remarkable advantage in terms of system complexity, the joint recovery of ($\mathbf{u}$, ϕ) is still complicated by the fact that the likelihood function does not take the classical form of a multivariate Gaussian probability density function due to the structure of the noise vector $\mathbf{w}$, which is not circularly symmetric. To overcome such a difficulty, for the time being we assume that $\mathbf{w}$ is a zero-mean circularly symmetric Gaussian (ZMCSG) complex vector with covariance matrix $\sigma_w^2 \mathbf{I}_{MP}$. Although this assumption holds true only in a perfectly balanced DCR architecture, it has been used even in the presence of non-negligible I/Q imbalances to derive novel frequency recovery schemes [26]. We point out that in our study the white noise assumption is adopted only to derive the CFO estimators and to analytically compute their accuracy, while the true noise statistics shown in (6) are employed in the numerical analysis to assess the system performance in a realistic scenario.

We start our analysis by rewriting (10) in a more compact form as

$$\mathbf{x} = \mathbf{A}(\phi)\mathbf{u} + \mathbf{w} \tag{14}$$

where the $(MP \times 2L)-$dimensional matrix $\mathbf{A}(\phi)$ is expressed by

$$\mathbf{A}(\phi) = [\boldsymbol{\Gamma}(\phi)\mathbf{G}_1\mathbf{C}\mathbf{G}_2 \ \ \boldsymbol{\Gamma}(-\phi)\mathbf{G}_1^*\mathbf{C}^*\mathbf{G}_2^*]. \tag{15}$$

Applying the ML estimation principle to the observation vector $\mathbf{x}$ under the ZMCSG assumption for $\mathbf{w}$, leads to the following maximization problem

$$\{\hat{\mathbf{u}}, \hat{\phi}\} = \arg\max_{\{\tilde{\mathbf{u}}, \tilde{\phi}\}} \left\{ -\left\| \mathbf{x} - \mathbf{A}(\tilde{\phi})\tilde{\mathbf{u}} \right\|^2 \right\}. \tag{16}$$

For a fixed value of $\tilde{\phi}$, the maximum is achieved at

$$\hat{\mathbf{u}}(\tilde{\phi}) = \left[\mathbf{A}^H(\tilde{\phi})\mathbf{A}(\tilde{\phi})\right]^{-1} \mathbf{A}^H(\tilde{\phi})\mathbf{x} \tag{17}$$

which, after substitution into (16), yields the CFO metric in the form

$$\Lambda\ (\tilde{\phi}) = \mathbf{x}^H \mathbf{A}(\tilde{\phi}) \left[\mathbf{A}^H(\tilde{\phi})\mathbf{A}(\tilde{\phi})\right]^{-1} \mathbf{A}^H(\tilde{\phi})\mathbf{x}. \tag{18}$$

It is worth noting that letting $L = P$ and replacing $\mathbf{G}_1\mathbf{C}\mathbf{G}_2$ in (15) with $\mathbf{1}_M \otimes \mathbf{I}_P$ leads to the JML estimator originally presented in [11], which was later applied to a repeated preamble in [23]. Compared to JML, the metric (18) exploits the mathematical structure of the received TP specified by the matrix $\mathbf{A}(\phi)$, which depends on the pilot symbols $\{c(n)\}$ and the DFT/IDFT matrices $\mathbf{G}_1$ and $\mathbf{G}_2$ as shown in (15). Accordingly, in the sequel the CFO estimator maximizing the metric (18) is referred to as the structured JML (SJML), i.e.

$$\hat{\phi}_{SJML} = \arg\max_{\tilde{\phi}} \{\Lambda(\tilde{\phi})\}. \tag{19}$$

TABLE I
COMPLEXITY OF THE INVESTIGATED SCHEMES

Algorithm	Number of flops	WLAN scenario
SJML	$16LMPN_\phi$	$1,572,864$
RC-SJML	$2LM(4P + 2M - 3) + 5N_\phi \log_2 N_\phi$	$11,872$
BLUE	$LM(8P + 3M - 4) + M/2$	$7,108$
CML	$(4MP - 3)(M - 1) + 5N_\phi \log_2 N_\phi$	$8,043$
JML	$8P(2M + 1)N_\phi$	$278,528$
RCE	$4(2MP + 1)L$	$6,168$

In order to assess the complexity of SJML, it is convenient to put (18) into the equivalent form

$$\Lambda\ (\tilde{\phi}) = \left\| \mathbf{L}_c^H(\tilde{\phi})\mathbf{A}^H(\tilde{\phi})\mathbf{x} \right\|^2 \tag{20}$$

where $\mathbf{L}_c(\tilde{\phi})\mathbf{L}_c^H(\tilde{\phi})$ is the Cholesky factorization of $\left[\mathbf{A}^H(\tilde{\phi})\mathbf{A}(\tilde{\phi})\right]^{-1}$. Then, we see that evaluating $\Lambda\ (\tilde{\phi})$ approximately needs $2LMP$ complex multiplications plus $2LMP$ complex additions for each value of $\tilde{\phi}$, which corresponds to $16LMP$ floating point operations (flops). In writing these figures we have borne in mind that a complex multiplication amounts to four real multiplications plus two real additions, while a complex additions is equivalent to two real additions. Furthermore, we have assumed that matrices $\mathbf{L}_c^H(\tilde{\phi})\mathbf{A}^H(\tilde{\phi})$ are pre-computed and stored in the receiver. The overall computational requirement of SJML is summarized in the first row of Table I, where we have denoted by N_ϕ the number of candidate values $\tilde{\phi}$. Since in the presence of a considerable CFO uncertainty the number N_ϕ can be quite large, we expect that SJML cannot be implemented with affordable complexity. This justifies the search for alternative schemes with less computational requirements and good estimation accuracy.

B. Reduced-Complexity CFO Estimation

We begin by partitioning vector $\mathbf{x}$ into M subvectors $\{\mathbf{x}_m; m = 0, 1, \ldots, M-1\}$, where $\mathbf{x}_m$ collects the P samples belonging to the mth received TP segment. Then, letting $\mathbf{x} = [\mathbf{x}_0^T \ \ \mathbf{x}_1^T \ \cdots \ \mathbf{x}_{M-1}^T]^T$ and bearing in mind (10) and (12), the mathematical model of $\mathbf{x}_m$ is found to be

$$\mathbf{x}_m = e^{jmP\phi}\boldsymbol{\Gamma}_P(\phi)\mathbf{F}_P\mathbf{C}\mathbf{G}_2\mathbf{h} + e^{-jmP\phi}\boldsymbol{\Gamma}_P(-\phi)\mathbf{F}_P^*\mathbf{C}^*\mathbf{G}_2^*\mathbf{q} + \mathbf{w}_m \tag{21}$$

where $\mathbf{w}_m$ is the mth subvector of $\mathbf{w} = [\mathbf{w}_0^T \ \ \mathbf{w}_1^T \ \cdots \ \mathbf{w}_{M-1}^T]^T$ and $\boldsymbol{\Gamma}_P(\phi) = \mathrm{diag}\{e^{jl\phi}, l = 0, 1, \ldots, P-1\}$. In order to simplify the SJML metric, we make the following approximation

$$\boldsymbol{\Gamma}_P(\phi) \simeq e^{j(P-1)\phi/2}\mathbf{I}_P \tag{22}$$

which amounts to replacing the linearly increasing phase shift $l\phi$ for $l = 0, 1, \ldots, P-1$ by its average value $(P-1)\phi/2$. Denoting by $|\phi|^{(\max)}$ the largest value of $|\phi|$, the maximum phase deviation between the entries of $\boldsymbol{\Gamma}_P(\phi)$ and $e^{j(P-1)\phi/2}\mathbf{I}_P$ turns out to be $(P-1)|\phi|^{(\max)}/2$. This suggests that approximation (22) becomes more and more questionable as P increases, and limits the range of P as discussed later in Sect. VI B.

Plugging (22) into (21) yields

$$\mathbf{x}_m \simeq e^{j(2mP+P-1)\phi/2}\mathbf{F}_P\mathbf{C}\mathbf{G}_2\mathbf{h} + e^{-j(2mP+P-1)\phi/2}\mathbf{F}_P^*\mathbf{C}^*\mathbf{G}_2^*\mathbf{q} + \mathbf{w}_m \quad (23)$$

which can also be rewritten in a more compact form as

$$\mathbf{x}_m = \mathbf{T}\mathbf{u}_m + \mathbf{w}_m \quad (24)$$

where $\mathbf{u}_m$ is a $2L-$dimensional vector expressed by

$$\mathbf{u}_m = \begin{bmatrix} e^{j(2mP+P-1)\phi/2}\mathbf{h} \\ e^{-j(2mP+P-1)\phi/2}\mathbf{q} \end{bmatrix} \quad (25)$$

and $\mathbf{T}$ is the following matrix of dimension $P \times (2L)$

$$\mathbf{T} = \begin{bmatrix}\mathbf{T}_1 \ \mathbf{T}_1^*\end{bmatrix} \quad (26)$$

with $\mathbf{T}_1 = \mathbf{F}_P\mathbf{C}\mathbf{G}_2$. From the simplified model (24), the ML estimate of $\mathbf{u}_m$ is computed as

$$\hat{\mathbf{u}}_m = (\mathbf{T}^H\mathbf{T})^{-1}\mathbf{T}^H\mathbf{x}_m. \quad (27)$$

Then, recalling the structure of $\mathbf{u}_m$ shown in (25), we observe that the first L elements of $\hat{\mathbf{u}}_m$ provide an estimate of $e^{j(2mP+P-1)\phi/2}\mathbf{h}$, while the last L elements provide an estimate of $e^{-j(2mP+P-1)\phi/2}\mathbf{q}$. Since in a practical scenario the energy of $\mathbf{q}$ is typically much smaller than the energy of $\mathbf{h}$, in the sequel we only exploit the first part of $\hat{\mathbf{u}}_m$ ($m = 0, 1, \ldots, M-1$) to retrieve the CFO. This approach has the remarkable advantage of reducing the system complexity without leading to any significant loss in estimation accuracy. Hence, substituting (24) into (27) and denoting by $\boldsymbol{\xi}_m$ the first L entries of $\hat{\mathbf{u}}_m$, we get

$$\boldsymbol{\xi}_m = e^{j(2mP+P-1)\phi/2}\mathbf{h}+\boldsymbol{\eta}_m \quad (28)$$

where $\boldsymbol{\eta}_m$ is a zero-mean Gaussian vector with covariance matrix $\mathbf{C}_\eta = \sigma_w^2\mathbf{K}$, and $\mathbf{K}$ is an $L-$dimensional matrix with entries $[\mathbf{K}]_{i,j} = [(\mathbf{T}^H\mathbf{T})^{-1}]_{i,j}$ for $1 \le i, j \le L$. Observing that

$$\mathbf{T}^H\mathbf{T} = \begin{bmatrix} \mathbf{T}_1^H\mathbf{T}_1 & \mathbf{T}_1^H\mathbf{T}_1^* \\ \mathbf{T}_1^T\mathbf{T}_1 & \mathbf{T}_1^T\mathbf{T}_1^* \end{bmatrix} \quad (29)$$

from the inversion formula of a partitioned matrix we have [27, p. 572]

$$\mathbf{K} = [\mathbf{T}_1^H\mathbf{T}_1 - \mathbf{T}_1^H\mathbf{T}_1^*(\mathbf{T}_1^T\mathbf{T}_1^*)^{-1}\mathbf{T}_1^T\mathbf{T}_1]^{-1}. \quad (30)$$

We now derive the joint ML estimate of the unknown parameters ($\mathbf{h}$,ϕ) starting from the observation vectors $\{\boldsymbol{\xi}_m; m = 0, 1, \ldots, M-1\}$. Neglecting irrelevant terms independent of ($\tilde{\mathbf{h}}, \tilde{\phi}$), we may write the log-likelihood function (LLF) in the form

$$\Psi\ (\tilde{\mathbf{h}}, \tilde{\phi}) = 2\Re\mathrm{e}\left\{\tilde{\mathbf{h}}^H\mathbf{K}^{-1}\sum_{m=0}^{M-1} e^{-j(2mP+P-1)\tilde{\phi}/2}\boldsymbol{\xi}_m\right\} - M(\tilde{\mathbf{h}}^H\mathbf{K}^{-1}\tilde{\mathbf{h}}). \quad (31)$$

Maximizing $\Psi\ (\tilde{\mathbf{h}}, \tilde{\phi})$ with respect to $\tilde{\mathbf{h}}$ yields

$$\hat{\mathbf{h}}(\tilde{\phi}) = \frac{1}{M}\sum_{m=0}^{M-1} e^{-j(2mP+P-1)\tilde{\phi}/2}\boldsymbol{\xi}_m \quad (32)$$

and plugging this result into (31) produces the concentrated likelihood function for the estimation of ϕ as

$$\Psi_c(\tilde{\phi}) = \left\| \sum_{m=0}^{M-1} e^{-jmP\tilde{\phi}}\mathbf{y}_m \right\|^2 \quad (33)$$

with $\mathbf{y}_m = \mathbf{K}^{-1/2}\boldsymbol{\xi}_m$. After some standard manipulations, we can put $\Psi_c(\tilde{\phi})$ in the equivalent form

$$\Psi_c(\tilde{\phi}) = \sum_{m=1}^{M-1} \Re\mathrm{e}\left\{R(m)e^{-jmP\tilde{\phi}}\right\} \quad (34)$$

where the quantities $\{R(m)\}$ are defined as

$$R(m) = \sum_{k=m}^{M-1} \mathbf{y}_{k-m}^H\mathbf{y}_k \quad 1 \le m \le M-1. \quad (35)$$

In the sequel, the CFO estimator maximizing $\Psi_c(\tilde{\phi})$ is referred to as the reduced-complexity SJML (RC-SJML), i.e.

$$\hat{\phi}_{RC-SJML} = \arg\max_{\tilde{\phi}}\{\Psi_c(\tilde{\phi})\}. \quad (36)$$

C. Remarks

1) Inspection of (34) reveals that $\Psi_c(\tilde{\phi})$ is periodic of period $2\pi/P$, meaning that the estimator provides ambiguous estimates unless ϕ is confined within the interval $|\phi| \le \pi/P$. Recalling the relationship (9) between ϕ and Δf, it turns out that the estimation range of RC-SJML is given by $|\Delta f| \le 1/(2PT_s)$.

2) The maximum of $\Psi_c(\tilde{\phi})$ can be found through the following two-step procedure. In the first step (coarse search), the CFO metric is evaluated over a set of $\tilde{\phi}$ values, say $\left\{\tilde{\phi}_n\right\}$, covering the uncertainty range of ϕ and the location $\tilde{\phi}_M$ of the maximum is determined over this set. In the second step (fine search), the quantities $\{\Psi_c(\tilde{\phi}_n)\}$ are interpolated to locate the local maximum nearest to $\tilde{\phi}_M$. The coarse search can be efficiently performed using Fast Fourier Transform (FFT) techniques. Specifically, we consider the following zero-padded sequence of length $N_\phi = M\gamma_{pr}$

$$R_{ZP}(m) = \begin{cases} R(m) & 1 \le m \le M-1 \\ 0 & M \le m \le N_\phi - 1 \ \text{ and } m = 0 \end{cases} \quad (37)$$

where $\gamma_{pr} \ge 1$ is an integer design parameter called *pruning factor*. Then, we compute the N_ϕ-point ($-N_\phi/2 < n \le N_\phi/2$) FFT of $R_{ZP}(m)$

$$\mathrm{FFT}\{R_{ZP}(m)\} = \sum_{m=0}^{N_\phi-1} R_{ZP}(m)e^{-j2\pi mn/N_\phi} \quad (38)$$

and observe that the real part of the FFT provides samples of the metric $\Psi_c(\tilde{\phi})$ evaluated at

$$\tilde{\phi}_n = \frac{2\pi n}{PM\gamma_{pr}}, \quad -N_\phi/2 < n \le N_\phi/2. \quad (39)$$

The maximum of the set $\{\Psi_c(\tilde{\phi}_n)\}$ is eventually sought, and this provides the coarse estimate of ϕ. From (39), it is seen that the pruning factor determines the granularity of the coarse search.

3) In assessing the complexity of RC-SJML, we observe that evaluating vectors $\mathbf{y}_m$ for $0 \le m \le M-1$ needs $8LMP - 2LM$ flops, while nearly $4LM(M-1)$ flops are required to obtain the correlations $R(m)$ for $1 \le m \le M-1$ starting from $\mathbf{y}_m$. Finally, the FFT of the sequence $R_{ZP}(m)$ is computed with $(N_\phi/2)\log_2(N_\phi)$ complex multiplications plus $N_\phi \log_2(N_\phi)$ complex additions, which corresponds to additional $5N_\phi \log_2(N_\phi)$ flops. The overall operations are summarized in the second row of Table I.

4) Evaluating $\hat{\mathbf{u}}_m$ as shown in (27) requires the invertibility of the $(2L)-$dimensional matrix $\mathbf{T}^H\mathbf{T}$, which is attainable only if $\mathbf{T}$ has full-rank $2L$. From (26), we see that rank($\mathbf{T}$) depends on $\mathbf{T}_1 = \mathbf{F}_P\mathbf{C}\mathbf{G}_2$ and, ultimately, on the structure of $\mathbf{C}$. In particular, when considering the short training sequence (STS) of the 802.11a preamble we have rank($\mathbf{T}$) = min $(2L, N_p)$, where $N_p = 12$ is the number of non-zero pilot symbols $\{c(n)\}$. In such a case, application of RC-SJML requires that $L \le N_p/2$, which poses a limit to the maximum channel order that can be handled. When such a constraint is not fulfilled, the problem arises as how to compute vector $\hat{\mathbf{u}}_m$. One possibility is to replace $(\mathbf{T}^H\mathbf{T})^{-1}$ in (27) by $(\mathbf{T}^H\mathbf{T}+\lambda\mathbf{I}_{2L})^{-1}$, where $\lambda > 0$ is a regularization parameter which ensures the invertibility of $\mathbf{T}^H\mathbf{T}+\lambda\mathbf{I}_{2L}$. A good choice for such a parameter is $\lambda = \sigma_w^2$, as in this case $\hat{\mathbf{u}}_m$ reduces to the minimum mean square error (MMSE) estimate of $\mathbf{u}_m$ based on the observation vector $\mathbf{x}_m$. Alternatively, we can replace the true channel order L by $\overline{L} = N_p/2$ for the sole purpose of evaluting $\hat{\mathbf{u}}_m$, and let the RC-SJML operate in a mismatched mode. In such a case, the estimation accuracy is expected to worsen more and more as the difference $L - \overline{L}$ grows large. This intuition will be checked later through numerical measurements.

IV. CFO Estimation in Closed-Form

Although RC-SJML can provide a remarkable reduction of the processing requirements with respect to SJML, the maximization problem in (36) still requires a search over the uncertainty range of ϕ, which may be cumbersome in certain applications. To overcome this problem, we introduce an alternative scheme that is able to estimate the CFO in closed-form. Our approach is based on some heuristic reasoning and exploits the correlations $\{R(m);\, 1 \le m \le M-1\}$ defined in (35).

We begin by deriving the mathematical model of vectors $\mathbf{y}_m = \mathbf{K}^{-1/2}\boldsymbol{\xi}_m$, with $\boldsymbol{\xi}_m$ as shown in (28). Letting

$$\mathbf{h}_{eq} = \mathbf{K}^{-1/2}\mathbf{h} \tag{40}$$

we get

$$\mathbf{y}_m = e^{j(2mP+P-1)\phi/2}(\mathbf{h}_{eq}+\mathbf{n}_m) \tag{41}$$

where $\mathbf{n}_m = \mathbf{K}^{-1/2}\boldsymbol{\eta}_m e^{-j(2mP+P-1)\phi/2}$ is a zero-mean Gaussian vector with covariance matrix $\mathbf{C}_n = \sigma_w^2\mathbf{I}_L$. Substituting this result into (35) produces

$$R(m) = (M-m)\left\|\mathbf{h}_{eq}\right\|^2 e^{jmP\phi}[1+\gamma(m)] \quad 1 \le m \le M-1 \tag{42}$$

with

$$\gamma(m) = \frac{1}{(M-m)\left\|\mathbf{h}_{eq}\right\|^2}\sum_{k=m}^{M-1}[\mathbf{h}_{eq}^H\mathbf{n}_k+\mathbf{n}_{k-m}^H\mathbf{h}_{eq}+\mathbf{n}_{k-m}^H\mathbf{n}_k]. \tag{43}$$

Inspection of (42) reveals that the unknown parameter ϕ is linearly related to the argument of $R(m)$. Hence, we define the angles

$$\theta(m) = \arg\{R(m)R^*(m-1)\} \quad 1 \le m \le H \tag{44}$$

where H is a design parameter not greater than $M-1$ and $R(0)$ is arbitrarily set to unity. Furthermore, we assume large SNR values such that $\arg\{1+\gamma(m)\} \simeq \gamma_I(m)$, with $\gamma_I(m)$ being the imaginary part of $\gamma(m)$. In these circumstances, from (42) we have

$$\theta(m) \simeq [P\phi + \gamma_I(m) - \gamma_I(m-1)]_{2\pi} \tag{45}$$

where $[x]_{2\pi}$ denotes the value of x reduced to the interval $[-\pi,\pi)$. If ϕ is adequately smaller than π/P, the quantity in brackets in (45) is (with high probability) less than π and $\theta(m)$ reduces to

$$\theta(m) = P\phi + \eta(m) \tag{46}$$

with $\eta(m) = \gamma_I(m) - \gamma_I(m-1)$. It is worth noting that the linear model (46) is exactly the same presented in [28] in the context of CFO recovery for OFDM receiver without any I/Q imbalance. The BLUE of ϕ as a function of the observation variables $\boldsymbol{\theta} = [\theta(1), \theta(2), \ldots, \theta(H)]^T$ is given by [27]

$$\hat{\phi}_{BLUE} = \frac{1}{P}\sum_{m=1}^{H}\alpha_{BLUE}(m)\theta(m) \tag{47}$$

where $\alpha_{BLUE}(m)$ is the mth element of

$$\boldsymbol{\alpha}_{BLUE} = \frac{\mathbf{C}_\eta^{-1}\mathbf{1}}{\mathbf{1}^T\mathbf{C}_\eta^{-1}\mathbf{1}} \tag{48}$$

and $\mathbf{C}_\eta$ is the covariance matrix of $\boldsymbol{\eta} = [\eta(1), \eta(2), \ldots, \eta(H)]^T$. The variance of $\hat{\phi}_{BLUE}$ is expressed by

$$\mathrm{var}(\hat{\phi}_{BLUE}) = \frac{1}{P^2}\frac{1}{\mathbf{1}^T\mathbf{C}_\eta^{-1}\mathbf{1}} \tag{49}$$

and depends on the design parameter H. In [28] it is shown that the minimum of var($\hat{\phi}_{BLUE}$) is achieved when $H = M/2$. In such a case we have

$$\alpha_{BLUE}(m) = 3\frac{4(M-m)(M-m+1)-M^2}{2M(M^2-1)} \tag{50}$$

and

$$\mathrm{var}(\hat{\phi}_{BLUE}) = \frac{6\sigma_w^2}{MP^2(M^2-1)\left\|\mathbf{h}_{eq}\right\|^2}. \tag{51}$$

The complexity of BLUE is assessed by observing that, besides the $8LMP - 2LM$ flops required to get vectors $\mathbf{y}_m$ for $0 \le m \le M-1$, additional $LM(3M-2) - M$ flops are involved in the evaluation of $R(m)$ for $1 \le m \le M/2$. The estimate $\hat{\phi}_{BLUE}$ is eventually obtained from the correlations $R(m)$ with $3M/2$ flops. This leads to the overall complexity listed in the third row of Table I.

$$\dot{\mathbf{B}}(\phi)=\begin{bmatrix}\mathbf{M} & \mathbf{0}\\ \mathbf{0} & \mathbf{M}\end{bmatrix}\begin{bmatrix}-\Im\text{m}\{\mathbf{A}_1(\phi)\} & -\Re\text{e}\{\mathbf{A}_1(\phi)\} & -\Im\text{m}\{\mathbf{A}_1(\phi)\} & \Re\text{e}\{\mathbf{A}_1(\phi)\}\\ \Re\text{e}\{\mathbf{A}_1(\phi)\} & -\Im\text{m}\{\mathbf{A}_1(\phi)\} & -\Re\text{e}\{\mathbf{A}_1(\phi)\} & -\Im\text{m}\{\mathbf{A}_1(\phi)\}\end{bmatrix} \tag{56}$$

V. CRB Analysis

It is interesting to compare the accuracy of the CFO estimation algorithms derived in the previous Sections with the relevant CRB. The latter is obtained starting from the signal model given in (14)-(15), and using the true noise statistics expressed in (6). We begin by arranging the received samples $\mathbf{x}$ into a real-valued vector $\check{\mathbf{x}}=[\mathbf{x}_I^T\ \mathbf{x}_Q^T]^T$, with $\mathbf{x}_I=\Re\text{e}\{\mathbf{x}\}$ and $\mathbf{x}_Q=\Im\text{m}\{\mathbf{x}\}$. Then, we define the real-valued CIR vector as $\check{\mathbf{u}}=[\mathbf{h}_{re}^T\ \mathbf{h}_{im}^T\ \mathbf{q}_{re}^T\ \mathbf{q}_{im}^T]^T$, where $\mathbf{h}_{re}$ and $\mathbf{q}_{re}$ are the real parts of $\mathbf{h}$ and $\mathbf{q}$, respectively, while $\mathbf{h}_{im}$ and $\mathbf{q}_{im}$ are the imaginary parts. Finally, letting $\check{\mathbf{w}}=[\mathbf{w}_I^T\ \mathbf{w}_Q^T]^T$, with $\mathbf{w}_I=\Re\text{e}\{\mathbf{w}\}$ and $\mathbf{w}_Q=\Im\text{m}\{\mathbf{w}\}$, we may rewrite (14) as

$$\check{\mathbf{x}}=\mathbf{B}(\phi)\check{\mathbf{u}}+\check{\mathbf{w}} \tag{52}$$

where

$$\mathbf{B}(\phi)=\begin{bmatrix}\Re\text{e}\{\mathbf{A}_1(\phi)\} & -\Im\text{m}\{\mathbf{A}_1(\phi)\} & \Re\text{e}\{\mathbf{A}_1(\phi)\} & \Im\text{m}\{\mathbf{A}_1(\phi)\}\\ \Im\text{m}\{\mathbf{A}_1(\phi)\} & \Re\text{e}\{\mathbf{A}_1(\phi)\} & -\Im\text{m}\{\mathbf{A}_1(\phi)\} & \Re\text{e}\{\mathbf{A}_1(\phi)\}\end{bmatrix} \tag{53}$$

with $\mathbf{A}_1(\phi)=\mathbf{\Gamma}(\phi)\mathbf{G}_1\mathbf{C}\mathbf{G}_2=\mathbf{\Gamma}(\phi)\,(\mathbf{1}_M\otimes\mathbf{T}_1)$. To proceed further, we denote by $\mathbf{C}_{\check{w}}$ the covariance matrix of the Gaussian vector $\check{\mathbf{w}}$, which can be computed through (6). Then, letting the set of unknown parameters be $\boldsymbol{\chi}=(\phi,\check{\mathbf{u}})$, it is found that the Fisher information matrix $\mathbf{\Omega}$ for the estimation of $\boldsymbol{\chi}$ takes the following form [27, Sec. 3.9]

$$\mathbf{\Omega}=\begin{bmatrix}\omega_{\phi\phi} & \boldsymbol{\omega}_{\phi\check{u}}^T\\ \boldsymbol{\omega}_{\phi\check{u}} & \mathbf{\Omega}_{\check{u}\check{u}}\end{bmatrix} \tag{54}$$

where

$$\begin{aligned}\omega_{\phi\phi}&=\check{\mathbf{u}}^T\dot{\mathbf{B}}^T(\phi)\mathbf{C}_{\check{w}}^{-1}\dot{\mathbf{B}}(\phi)\check{\mathbf{u}}\\ \boldsymbol{\omega}_{\phi\check{u}}&=\mathbf{B}^T(\phi)\mathbf{C}_{\check{w}}^{-1}\dot{\mathbf{B}}(\phi)\check{\mathbf{u}}\\ \mathbf{\Omega}_{\check{u}\check{u}}&=\mathbf{B}^T(\phi)\mathbf{C}_{\check{w}}^{-1}\mathbf{B}(\phi)\end{aligned} \tag{55}$$

and we have denoted by $\dot{\mathbf{B}}(\phi)$ the derivative of $\mathbf{B}(\phi)$ with respect to ϕ. Taking (53) into account, yields (56), as shown at the top of this page, with $\mathbf{M}=\text{diag}\{0,1,\ldots,MP-1\}$. The CRB for the estimation of ϕ is the $(1,1)$th entry of $\mathbf{\Omega}^{-1}$, i.e.

$$\text{CRB}(\phi)=\frac{1}{\omega_{\phi\phi}-\boldsymbol{\omega}_{\phi\check{u}}^T\mathbf{\Omega}_{\check{u}\check{u}}^{-1}\boldsymbol{\omega}_{\phi\check{u}}} \tag{57}$$

while the CRBs for the estimation of the entries of $\check{\mathbf{u}}$ are the diagonal elements of the following matrix

$$\mathbf{J}=\mathbf{\Omega}_{\check{u}\check{u}}^{-1}+\frac{\mathbf{\Omega}_{\check{u}\check{u}}^{-1}\boldsymbol{\omega}_{\phi\check{u}}\boldsymbol{\omega}_{\phi\check{u}}^T\mathbf{\Omega}_{\check{u}\check{u}}^{-1}}{\omega_{\phi\phi}-\boldsymbol{\omega}_{\phi\check{u}}^T\mathbf{\Omega}_{\check{u}\check{u}}^{-1}\boldsymbol{\omega}_{\phi\check{u}}}. \tag{58}$$

The *normalized* CRBs for the estimation of $\mathbf{h}$ and $\mathbf{q}$ are eventually given by

$$\text{CRB}(\mathbf{h})=\frac{1}{\|\mathbf{h}\|^2}\sum_{m=1}^{2L}[\mathbf{J}]_{m,m} \tag{59}$$

and

$$\text{CRB}(\mathbf{q})=\frac{1}{\|\mathbf{q}\|^2}\sum_{m=2L+1}^{4L}[\mathbf{J}]_{m,m}. \tag{60}$$

Unfortunately, (57) does not provide any clear indication about the impact of the system parameters on the ultimate accuracy achievable in the CFO estimation process. A more useful expression can be found by evaluating an approximate version of the CRB. The latter is obtained from the simplified model of the M vectors $\{\boldsymbol{\xi}_m; m=0,1,\ldots,M-1\}$ given in (28), combined with the white Gaussian noise assumption. Skipping the details for space limitations, the approximate CRB (ACRB) is found to be

$$\text{ACRB}\{\phi\}=\frac{6\sigma_w^2}{MP^2(M^2-1)\left\|\mathbf{h}_{eq}\right\|^2} \tag{61}$$

and coincides with $\text{var}(\hat{\phi}_{BLUE})$ given in (51).

VI. Simulation Results

A. Simulation Model

Computer simulations are conducted to examine the performance of the proposed methods in an OFDM WLAN system compliant with the IEEE 802.11a standard [1]. The DFT size is $N=64$, while the sampling interval is set to $T_s=50$ ns. This corresponds to a transmission bandwidth of 20 MHz with a subcarrier distance of 312.5 kHz. The synchronization schemes are applied to the STS placed in front of each frame. This sequence carries $N_p=12$ non-zero pilot symbols, and is divided into $M_T=10$ repeated parts, each containing $P=16$ samples. After discarding the first two segments as the CP of the TP, the remaining $M=8$ segments are exploited for CFO recovery. Hence, throughout simulations we let $P=16$ and $M=8$ unless otherwise specified. We adopt a discrete-time channel model and collect the samples of $v(t)$ into a vector $\mathbf{v}=[v(0),v(1),\ldots,v(L_v-1)]^T$ of order L_v. The entries of $\mathbf{v}$ follow a circularly-symmetric Gaussian distribution with an exponentially decaying power delay profile

$$\text{E}\{|v(k)|^2\}=\sigma_v^2\exp(-k/L_v)\quad k=0,1,\ldots,L_v-1 \tag{62}$$

where $L_v=4$ (with the only exception of Fig. 9) and σ_v^2 is chosen such that $\text{E}\{\|\mathbf{v}\|^2\}=1$. Both frequency independent and frequency selective RF imperfections are considered. If not otherwise stated, the LO-induced imbalance is characterized by $\alpha=1$ dB and $\psi=5$ degrees. The receive I/Q filters have discrete-time impulse responses $\mathbf{g}_I=[0,1,\mu]^T$ and $\mathbf{g}_Q=[\mu,1,0]^T$ with $\mu=0.1$, which results into overall CIRs $h[k]$ and $q[k]$ having support $k=0,1,\ldots,L-1$, with $L=L_v+2$. These values have been previously adopted in the related literature [11] and represent a plausible model for I/Q mismatches. In addition to the aforementioned simulation set-up, in our study we also consider a more general scenario

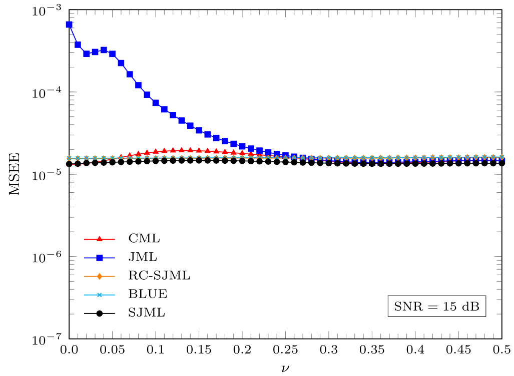

Fig. 2. Accuracy of the CFO estimators vs. ν with SNR = 15 dB.

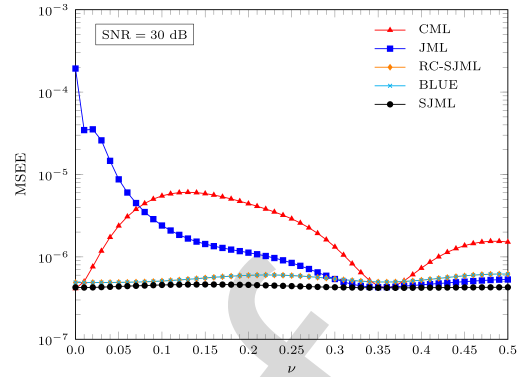

Fig. 3. Accuracy of the CFO estimators vs. ν with SNR = 30 dB.

wherein a coefficient $\rho \in [0, 4]$ is used to specify the values of the I/Q imbalance parameters as $\mu = 0.1\rho$, $\alpha = 1+0.122\rho$ and $\psi = 5\rho$ degrees. This allows us to assess the sensitivity of the considered schemes to the amount of RF imperfections, with $\rho = 0$ corresponding to an ideal situation where no I/Q imbalance is present.

Assuming a carrier frequency of 5 GHz and an oscillator instability of ±30 parts-per-million (ppm), we obtain $|\phi|^{(\max)} = 0.015\pi$. This value falls well within the estimation range of the RC-SJML and BLUE, which is given by $|\phi| \le \pi/P = 0.0625\pi$. When using SJML and RC-SJML, parameter N_ϕ is set to 128 since numerical simulations indicate that no significant improvement is achieved with $N_\phi > 128$.

B. Performance Assessment

The accuracy of the proposed frequency recovery schemes is assessed in terms of their mean square estimation error (MSEE). The estimated parameter is the CFO normalized by the subcarrier spacing, which is defined as $\nu = NT_s\Delta f$ or, equivalently, $\nu = N\phi/(2\pi)$. Recalling that $|\phi|^{(\max)} = 0.015\pi$, the uncertainty range of ν is given by $|\nu| \le 0.48$. Comparisons are made with alternative ML-oriented methods, including the CML [24] and JML [11]. The complexity of these estimators has been evaluated in [23] and is reported in Table I. In writing these results we have borne in mind that the coarse search with CML can be efficiently performed through FFT techniques, while a similar approach cannot be adopted with JML.

Fig. 2 illustrates the MSEE of the CFO estimators as a function of ν measured at SNR=15 dB. We see that JML performs poorly for small CFO values, while the accuracy of the other schemes depends weakly on ν. The reason for the poor performance of JML when ν approaches zero is that this scheme aims at jointly estimating the channel distorted signal component $\mathbf{a} = \mathbf{\Gamma}_P(\phi)\mathbf{F}_P\mathbf{C}\mathbf{G}_2\mathbf{h}$ and its mirror image $\mathbf{b} = \mathbf{\Gamma}_P(-\phi)\mathbf{F}_P^*\mathbf{C}^*\mathbf{G}_2^*\mathbf{q}$ without effectively exploiting their mathematical model. Since in the absence of any CFO the mth received TP segment in (21) becomes $\mathbf{x}_m = \mathbf{a}+\mathbf{b}+\mathbf{w}_m$, there is no possibility for JML to get individual estimates of $\mathbf{a}$ and $\mathbf{b}$ in this specific situation. In contrast, the proposed algorithms can work satisfactorily for any CFO value as they exploit the inherent structure of $\mathbf{a}$ and $\mathbf{b}$, which makes these vectors resolvable even when $\nu = 0$. It is worth observing that CML,

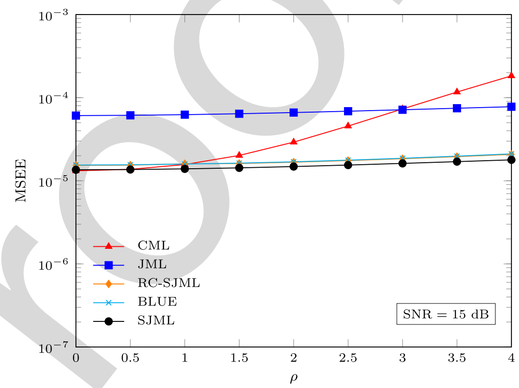

Fig. 4. Accuracy of the CFO estimators vs. ρ with SNR = 15 dB.

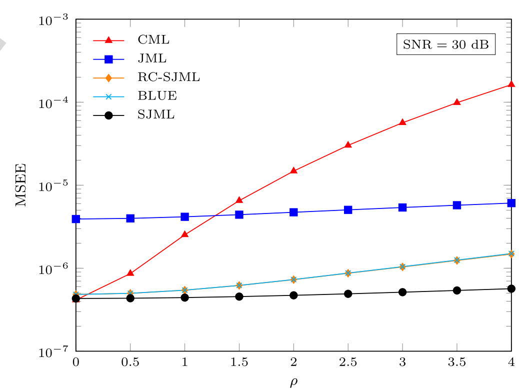

Fig. 5. Accuracy of the CFO estimators vs. ρ with SNR = 30 dB.

which is derived by ignoring the presence of I/Q imbalances, performs remarkably better than JML for $\nu < 0.15$. We also see that the accuracy of RC-SJML and BLUE is virtually the same as that of SJML, in spite of their reduced complexity.

The results of Fig. 3 are obtained under the same operating conditions of Fig. 2, except that the SNR is now set to 30 dB. In such a case, the performance of CML exhibits large fluctuations as a function of ν, while the proposed schemes provide a remarkable accuracy irrespective of the CFO value. Again, JML performs poorly when ν approaches zero due to the impossibility of resolving vectors $\mathbf{a}$ and $\mathbf{b}$.

Figs. 4 and 5 show the MSEE of the CFO estimators as a function of ρ with ν uniformly distributed over the

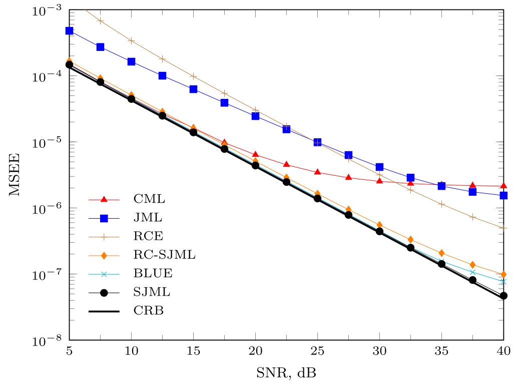

Fig. 6. Accuracy of the CFO estimators vs. SNR.

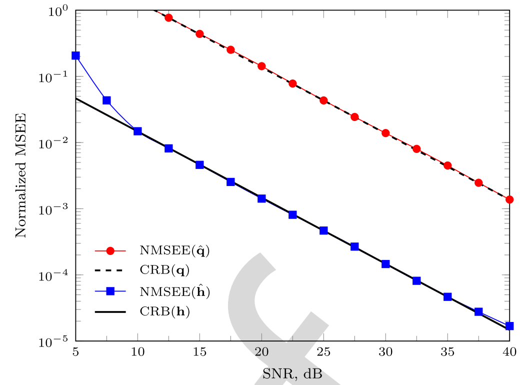

Fig. 7. Accuracy of the CIR estimates vs. SNR.

interval $[-0.5, 0.5]$. The SNR is 15 dB in Fig. 4 and 30 dB in Fig. 5. These results indicate that, irrespective of the SNR, the accuracy of JML and SJML is virtually independent of ρ, while CML is significantly affected by the amount of I/Q imbalances. As for RC-SJML and BLUE, they exhibit a remarkable resilience against RF imperfections at an SNR of 15 dB, while some performance degradation is observed at SNR $= 30$ dB in the presence of severe I/Q mismatches. However, these schemes largely outperform both JML and CML, while exhibiting a tolerable loss with respect to SJML.

Fig. 6 illustrates the accuracy of the investigated schemes as a function of the SNR when $\rho = 1$ and ν varies uniformly within the interval $[-0.5, 0.5]$. The curve labeled CRB corresponds to the bound reported in (57) and it is shown as a benchmark. Comparisons are also made with the reduced-complexity estimator (RCE) proposed in [25]. Although RCE was originally designed to operate with a TP composed of two identical halves, it can be applied to the 802.11a STS as well by considering such a sequence as the concatenation of two repeated segments $[\mathbf{x}_0^T \ \mathbf{x}_1^T \cdots \mathbf{x}_{M/2-1}^T]^T$ and $[\mathbf{x}_{M/2}^T \ \mathbf{x}_{M/2+1}^T \cdots \mathbf{x}_{M-1}^T]^T$. We see that SJML attains the CRB at any SNR value. Both RC-SJML and BLUE perform similarly to SJML (apart for a negligible loss in the high SNR region) and achieve a substantial gain with respect to JML and RCE. As for the CML curve, it keeps close to the CRB when SNR$<$15 dB, while it is plagued by a considerable floor at larger SNR values. Since our numerical analysis did not reveal any tangible difference between the true CRB and its approximation (61), we conclude that the noise term $w(t)$ in (2) can reasonably be modeled as a circularly symmetric white Gaussian process.

The accuracy of the estimated CIR vectors at different SNR values is assessed in Fig. 7 using the normalized MSEE (NMSEE) of $\hat{\mathbf{h}}$ and $\hat{\mathbf{q}}$, which is defined as

$$\mathrm{NMSEE}(\hat{\mathbf{h}}) = \frac{\mathrm{E}\left\{\left\|\hat{\mathbf{h}} - \mathbf{h}\right\|^2\right\}}{\mathrm{E}\{\|\mathbf{h}\|^2\}},$$

$$\mathrm{NMSEE}(\hat{\mathbf{q}}) = \frac{\mathrm{E}\left\{\left\|\hat{\mathbf{q}} - \mathbf{q}\right\|^2\right\}}{\mathrm{E}\{\|\mathbf{q}\|^2\}}. \tag{63}$$

Here, the estimate $\hat{\mathbf{u}} = [\hat{\mathbf{h}}^T \ \hat{\mathbf{q}}^T]^T$ is obtained as indicated in (17) letting $\tilde{\phi} = \hat{\phi}_{BLUE}$ and using the same operating scenario of Fig. 6. At medium and large SNR values, we see that both curves are tight to the relevant CRBs given in (59) and (60), while a certain discrepancy occurs in the low SNR region.

In order to assess the extent to which the approximation (22) can reasonably be adopted, it is interesting to investigate the impact of parameter P on the accuracy of the CFO estimate. For this purpose, in Fig. 8 we show the MSEE of the BLUE as a function of the SNR for $P = 16$, 32 and 64. Since the length of the TP is fixed to $MP = 128$, the corresponding values of M are 8, 4 and 2. In particular, the case $P = 32$ is handled by viewing the 802.11a STS as the concatenation of four repeated parts $[\mathbf{x}_0^T \ \mathbf{x}_1^T]^T$, $[\mathbf{x}_2^T \ \mathbf{x}_3^T]^T$, $[\mathbf{x}_4^T \ \mathbf{x}_5^T]^T$ and $[\mathbf{x}_6^T \ \mathbf{x}_7^T]^T$, with each vector $\mathbf{x}_i$ being composed of 16 elements, while the case $P = 64$ is tackled by dividing the TP into two parts $[\mathbf{x}_0^T \ \mathbf{x}_1^T \ \mathbf{x}_2^T \ \mathbf{x}_3^T]^T$ and $[\mathbf{x}_4^T \ \mathbf{x}_5^T \ \mathbf{x}_6^T \ \mathbf{x}_7^T]^T$. It turns out that, at SNR values smaller than 30 dB, the MSEE is practically the same with either $P = 16$ or 32, and keeps close to the relevant CRB given in (57). In contrast, very poor estimates are obtained with $P = 64$. It is worth noting that the formidable performance degradation incurred by the BLUE in passing from $P = 32$ to 64 cannot be totally ascribed to the approximation (22). Indeed, when $P = 64$ the estimation range of RC-SJML and BLUE is reduced to $|\phi| \leq 0.015625\pi$, which is only marginally greater than the value $|\phi|^{(\max)} = 0.015\pi$ adopted throughout simulations. In the presence of noise, we expect that the phase term $\theta(m)$ defined in (45) may occasionally experience jumps of 2π when $P\phi$ is close to $\pm\pi$ as a consequence of the wrapping phenomenon. Our analysis confirms the presence of these jumps when $P = 64$, which justifies the impressive loss of performance exhibited by the BLUE in this specific situation.

The results of Fig. 8 provide useful information about the maximum value of P that can be used with the BLUE. To see how this happens, we recall that the maximum phase error between $\mathbf{\Gamma}_P(\phi)$ and its approximation $e^{j(P-1)\phi/2}\mathbf{I}_P$ is $\Delta\phi^{(\max)} = (P-1)\,|\phi|^{(\max)}/2$. On the other hand, the MSEE curves in Fig. 8 indicate that, compared to the case $P = 16$, no penalty in estimation accuracy occurs when $P = 32$ and $|\phi|^{(\max)} = 0.015\pi$, yielding $\Delta\phi^{(\max)} \simeq \pi/4$. This means that a sufficient condition for applying the BLUE without incurring significant performance degradation

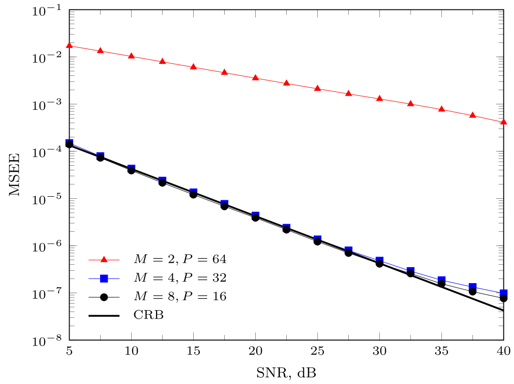

Fig. 8. Accuracy of the BLUE vs SNR for different values of P and $MP = 128$.

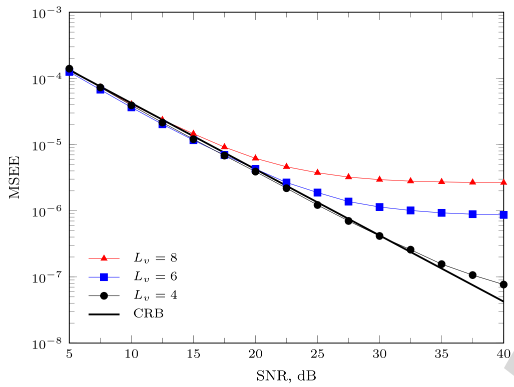

Fig. 9. Accuracy of the BLUE vs. SNR for different values of the channel order.

is $(P-1)\,|\phi|^{(\max)}/2 \le \pi/4$, which limits the range of P to

$$P \le 1 + \frac{\pi}{2|\phi|^{(\max)}}. \tag{64}$$

Fig. 9 illustrates the impact of the channel length on the performance of the BLUE when the constraint $L \le N_p/2$ is not fulfilled. In these simulations, the MSEE curves are obtained by designing the BLUE for a fictitious channel order $\overline{L_\upsilon} = 4$, (corresponding to $\overline{L} = \overline{L_\upsilon} + 2 = 6$), while the true values of L_υ are 4, 6 and 8. As expected, in the high SNR region the estimation accuracy exhibits an irreducible floor, which increases with the difference $L_\upsilon - \overline{L_\upsilon}$. On the other hand, all the curves attain the CRB when the SNR is smaller than 15 dB, thereby revealing an adequate resilience against a possible mismatch in the channel order.

We complete our analysis by comparing the investigated CFO recovery schemes in terms of their computational complexity. The last column of Tab. I shows the number of required flops when the algorithms are applied to a WLAN scenario with $P = 16$ and $M = 8$. Based on these results, we observe that SJML is hardly implementable due to its prohibitive complexity. A similar conclusion applies to JML which, in spite of its large computational load, provides poor performance when compared to BLUE and RC-SJML. Hence, leaving aside the SJML and JML, in Fig. 10 we report the number of flops required by the other explored schemes as a function of P. The curves are obtained by substituting

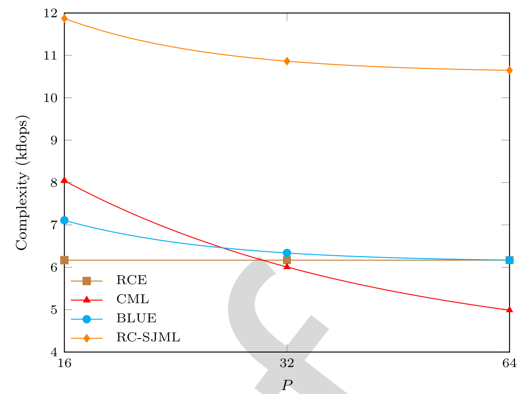

Fig. 10. Complexity of RC-SJML, BLUE, RCE and CML vs. P with $MP = 128$.

$MP = 128$, $L = 6$, and $N_\phi = 128$ in the expressions given in Tab. I. As is seen, the processing load of RCE is independent of P, while the complexity of the other algorithms decreases with P. These results indicate that the improved performance of RC-SJML with respect to existing alternatives (CML and RCE) is obtained at the price of an increase of the processing requirement by a factor of two. On the other hand, the BLUE attains the accuracy of RC-SJML with a computational load that is nearly the same as that of CML and RCE with either $P = 16$ or $P = 32$. Combining the MSEE measurements of Fig. 8 with the complexity analysis of Fig. 10, we conclude that $P = 32$ (and $M = 4$) is a good design choice when the BLUE is applied to a WLAN system compliant with the 802.11a standard.

VII. Conclusions

We analyzed the CFO estimation problem in an OFDM receiver plagued by frequency-selective I/Q imbalances. In doing so, we assumed that a repeated training preamble is available in front of each data packet to assist the synchronization task. Our first objective was the joint ML estimation of the CFO and channel impulse responses of the direct signal component and its mirror image. By exploiting knowledge of the pilot symbols embedded in the preamble, we derived a novel scheme (SJML) which eliminates the sign ambiguity problem of the JML estimator. Since implementation of SJML is impractical, we derived two alternative reduced-complexity schemes (RC-SJML and BLUE) by neglecting the phase rotation induced by the CFO within each TP segment. Upon considering a practical scenario compliant with the 802.11a WLAN standard, the following results were found: 1) both RC-SJML and BLUE lead to a drastic reduction of the processing load with respect to SJML without incurring any significant penalty in estimation accuracy; 2) compared to existing alternatives (CML, RCE, JML), RC-SJML exhibits a remarkable improvement of the system performance at the price of a certain increase of the computational load with respect to CML and RCE; 3) the BLUE attains the same performance of RC-SJML, while exhibiting a complexity similar to that of CML and RCE; 4) the length of the repetitive TP segment must be carefully designed in order to achieve a good trade-off between estimation accuracy, system complexity, and estimation range.

These conclusions indicate that the BLUE represents a practical solution for accurate CFO recovery in an OFDM direct-conversion receiver.

REFERENCES

[1] *Wireless LAN Medium Access Control (MAC) and Physical Layer (PHY) Specifications, Higher Speed Physical Layer Extension in the 5 GHz Band*, IEEE Standard 802.11 WG, Sep. 1999.

[2] *IEEE Standard for Local and Metropolitan Area Networks, Part16: Air Interface for Fixed and Mobile Broadband Wireless Access Systems*, IEEE Standard 802.16, 2004.

[3] *Evolved Universal Terrestrial Radio Access (E-UTRA); Physical Channels and Modulation*, document 3GPP TS 36.211, 2012.

[4] W. Namgoong and T. H. Meng, "Direct-conversion RF receiver design," *IEEE Trans. Commun.*, vol. 49, no. 3, pp. 518–529, Mar. 2001.

[5] M. Valkama, M. Renfors, and V. Koivunen, "Advanced methods for I/Q imbalance compensation in communication receivers," *IEEE Trans. Signal Process.*, vol. 49, no. 10, pp. 2335–2344, Oct. 2001.

[6] F. Yan, W.-P. Zhu, and M. O. Ahmad, "Carrier frequency offset estimation for OFDM systems with I/Q imbalance," in *Proc. 47th IEEE Midwest Symp. Circuits Syst. (MWSCAS)*, vol. 2. Jul. 2004, pp. 633–636s.

[7] L. Lanante, Jr., M. M. Kurosaki, and H. Ochi, "Low complexity compensation of frequency dependent I/Q imbalance and carrier frequency offset for direct conversion receivers," in *Proc. IEEE Int. Symp. Circuits Syst. (ISCAS)*, Jun. 2010, pp. 2067–2070.

[8] S. D. Rore, E. Lopez-Estraviz, F. Horlin, and L. van der Perre, "Joint estimation of carrier frequency offset and IQ imbalance for 4G mobile wireless systems," in *Proc. Int. Conf. Commun. (ICC)*, vol. 5. Jun. 2006, pp. 2066–2071.

[9] Y.-C. Pan and S.-M. Phoong, "A new algorithm for carrier frequency offset estimation in the presence of I/Q imbalance," in *Proc. IEEE Veh. Techn. Conf. (VTC-Spring)*, Apr. 2010, pp. 1–5.

[10] M. Morelli and M. Moretti, "Carrier frequency offset estimation for OFDM direct-conversion receivers," *IEEE Trans. Wireless Commun.*, vol. 11, no. 7, pp. 2670–2679, Jul. 2012.

[11] G. Xing, M. Shen, and H. Liu, "Frequency offset and I/Q imbalance compensation for direct-conversion receivers," *IEEE Trans. Wireless Commun.*, vol. 4, no. 2, pp. 673–680, Mar. 2005.

[12] J. Park, Y. Lee, and H. Park, "Preamble design for joint estimation of CFO and I/Q imbalance for direct conversion OFDM system," *IET Commun.*, vol. 3, no. 4, pp. 597–602, 2009.

[13] C. J. Hsu, R. Cheng, and W. H. Sheen, "Joint least squares estimation of frequency, DC offset, I-Q imbalance, and channel in MIMO receivers," *IEEE Trans. Veh. Technol.*, vol. 58, no. 5, pp. 2201–2213, Jun. 2009.

[14] X. Cai, Y.-C. Wu, H. Lin, and K. Yamashita, "Estimation and compensation of CFO and I/Q imbalance in OFDM systems under timing ambiguity," *IEEE Trans. Vehic. Techn.*, vol. 60, no. 3, pp. 1200–1205, Mar. 2011.

[15] H. Lin, X. Zhu, and K. Yamashita, "Low-complexity pilot-aided compensation for carrier frequency offset and I/Q imbalance," *IEEE Trans. Commun*, vol. 58, no. 2, pp. 448–452, Feb. 2010.

[16] Y. C. Pan and S. M. Phoong, "A time-domain joint estimation algorithm for CFO and I/Q imbalance in wideband direct-conversion receivers," *IEEE Trans. Wireless Commun.*, vol. 11, no. 7, pp. 2353–2361, Jul. 2012.

[17] X. Wang, Y. Xue, L. Liu, F. Ye, and J. Ren, "Carrier frequency offset estimation in the presence of I/Q mismatch for wideband OFDM systems," in *Proc. IEEE 55th Int. Symp. Circuits Syst. (MWSCAS)*, Aug. 2012, pp. 924–927.

[18] R. Kume, H. Lin, and K. Yamashita, "Repeated preamble based carrier frequency offset estimation in the presence of I/Q imbalance," in *Proc. IEEE Int. Conf. Commun. (ICC)*, Jun. 2012, pp. 4867–4871.

[19] M. Morelli and H. Lin, "ESPRIT-based carrier frequency offset estimation for OFDM direct-conversion receivers," *IEEE Commun. Lett.*, vol. 17, no. 8, pp. 1513–1516, Aug. 2013.

[20] M. Morelli and M. Moretti, "A SAGE approach to frequency recovery in OFDM direct-conversion receivers," *IEEE Commun. Lett.*, vol. 18, no. 4, pp. 536–539, Apr. 2014.

[21] U. Tureli, H. Liu, and M. Zoltowski, "OFDM blind carrier offset estimation: ESPRIT," *IEEE Trans. Commun.*, vol. 48, no. 9, pp. 1459–1461, Sep. 2000.

[22] J. A. Fessler and A. O. Hero, "Space-alternating generalized expectation-maximization algorithm," *IEEE Trans. Signal Process.*, vol. 42, no. 10, pp. 2664–2677, Oct. 1994.

[23] A. A. D'Amico, L. Marchetti, M. Morelli, and M. Moretti, "Frequency estimation in OFDM direct-conversion receivers using a repeated preamble," *IEEE Trans. Commun*, vol. 64, no. 3, pp. 1246–1258, Mar. 2016.

[24] M. Ghogho, A. Swami, and P. Ciblat, "Training design for CFO estimation in OFDM over correlated multipath fading channels," in *Proc. Global Telecommun. Conf. (GLOBECOM)*, Nov. 2007, pp. 2821–2825.

[25] M. Asim, M. Ghogho, and D. McLernon, "OFDM receiver design in the presence of frequency selective I/Q imbalance and CFO," in *Proc. 21st Eur. Signal Process. Conf. (EUSIPCO)*, Marrakesh, Morocco, Sep. 2013, pp. 1–5.

[26] G.-T. Gil, I.-H. Sohn, J.-K. Park, and Y. H. Lee, "Joint ML estimation of carrier frequency, channel, I/Q mismatch, and DC offset in communication receivers," *IEEE Trans. Veh. Technol.*, vol. 54, no. 1, pp. 338–349, Jan. 2005.

[27] S. M. Kay, *Fundamentals of Statistical Signal Processing: Estimation Theory*. Englewood Cliffs, NJ, USA: Prentice-Hall, 1993.

[28] M. Morelli and U. Mengali, "An improved frequency offset estimator for OFDM applications," *IEEE Commun. Lett.*, vol. 3, no. 3, pp. 75–77, Mar. 1999.

Antonio A. D'Amico received the Dr.Ing. degree in electronic engineering and the Ph. D. degree from the University of Pisa, Italy, in 1992 and 1997, respectively. He is currently an Associate Professor with the Department of Information Engineering, University of Pisa. His research interests are in digital communication theory, with emphasis on synchronization algorithms, channel estimation, and detection techniques.

Michele Morelli received the Laurea degree *(cum laude)* in electrical engineering from the University of Pisa, Italy, in 1991, and the Ph.D. degree in electrical engineering from the University of Pisa. From 1992 to 1995, he was with the Department of Information Engineering, University of Pisa. In 1996, he joined the Centro Studi Metodi e Dispositivi per Radiotrasmissioni, Italian National Research Council, Pisa, where he was a Research Assistant. Since 2001, he has been with the Department of Information Engineering, University of Pisa, where he is a Professor of telecommunications. His research interests are in wireless communication theory, with emphasis on synchronization algorithms and channel estimation in multiple-access communication systems. He was a co-recipient of the VTC2006 (Fall) Best Student Paper Award. He has served as an Associate Editor for the IEEE TRANSACTIONS ON WIRELESS COMMUNICATIONS and the IEEE WIRELESS COMMUNICATION LETTERS. He is currently serving as an Associate Editor for the IEEE TRANSACTIONS ON COMMUNICATIONS.

Marco Moretti (M'03) received the degree in electronic engineering from the University of Florence, Florence, Italy, in 1995, and the Ph.D. degree from the Delft University of Technology, Delft, The Netherlands, in 2000. From 2000 to 2003, he was a Senior Researcher with Marconi Mobile. He is currently an Assistant Professor with the University of Pisa, Pisa, Italy. His research interests include resource allocation for multicarrier systems, synchronization, and channel estimation. He is an Associate Editor of the IEEE TRANSACTIONS ON SIGNAL PROCESSING.

Periodic Preamble-Based Frequency Recovery in OFDM Receivers Plagued by I/Q Imbalance

Antonio A. D'Amico, Michele Morelli, *Senior Member, IEEE*, and Marco Moretti, *Member, IEEE*

***Abstract*— The direct conversion receiver (DCR) architecture has received much attention in the last few years as an effective means to obtain user terminals with reduced cost, size, and power consumption. A major drawback of a DCR device is the possible insertion of in-phase/quadrature imbalances in the demodulated signal, which can seriously degrade the performance of conventional synchronization algorithms. In this paper, we investigate the problem of carrier frequency offset (CFO) recovery in an orthogonal frequency-division multiplexing receiver equipped with a DCR front-end. Our approach is based on maximum likelihood (ML) arguments and aims at jointly estimating the CFO, the useful signal component, and its mirror image. In doing so, we exploit knowledge of the pilot symbols transmitted within a conventional repeated training preamble appended in front of each data packet. Since the exact ML solution turns out to be too complex for practical purposes, we propose two alternative schemes which can provide nearly optimal performance with substantial computational saving. One of them provides the CFO in closed-form, thereby avoiding any grid-search procedure. The accuracy of the proposed methods is assessed in a scenario compliant with the 802.11a WLAN standard. Compared to existing solutions, the novel schemes achieve improved performance at the price of a tolerable increase of the processing load.**

***Index Terms*— Carrier frequency estimation, OFDM, direct-conversion receiver, I/Q imbalance.**

I. Introduction

ORTHOGONAL frequency-division multiplexing (OFDM) is a popular multicarrier technology which offers remarkable resilience against multipath distortions, increased spectral efficiency, and the possibility of performing adaptive modulation and coding. Due to such potential advantages, it has been adopted in several wideband commercial systems, including the IEEE 802.11a wireless local area network (WLAN) [1], the IEEE 802.16 wireless metropolitan area network (WMAN) [2], and the 3GPP long-term evolution (LTE) [3]. Recent studies indicate that the use of a direct-conversion receiver (DCR) in combination with the OFDM technology can provide an effective means for the implementation of user terminals with reduced size and power consumption [4]. These advantages are achieved through elimination of expensive intermediate frequency (IF) filters and other off-chip components employed in the classical superheterodyne architecture. The price is a higher degree of radio-frequency (RF) imperfections arising from the use of analog in-phase/quadrature (I/Q) low-pass filters (LPF) with mismatched frequency responses, and from local oscillator (LO) signals with amplitude and phase imbalances. In general, LO-induced distortions are nearly flat in the frequency domain, while filter mismatches can vary substantially over the signal bandwidth, especially in a wideband communication system [5]. If not properly compensated, the I/Q imbalance introduces image interference from mirrored subcarriers, with ensuing limitations of the system performance. In addition to I/Q imperfections, an OFDM receiver is also vulnerable to the carrier frequency offset (CFO) between the incoming waveform and the LO signals, which generates interchannel interference in the demodulated signal.

In recent years, an intense research activity has been conducted to investigate the problem of CFO recovery in OFDM systems plagued by frequency-selective I/Q imperfections. Many available solutions operate in the time-domain and exploit a suitably designed training preamble (TP) appended in front of the data packet. For example, the authors of [6] and [7] recover the cosine of the CFO by using a TP composed of three repeated segments. However, due to the even property of the cosine function, the estimated frequency is affected by a inherent sign ambiguity, which severely limits the accuracy in case of small CFO values. Some feasible solutions to fix the sign ambiguity problem are presented in [8]–[10], where the original TP of [6] is properly extended so as to retrieve both the cosine and the sine of the CFO. Unambiguous frequency estimates are also obtained in [11] and [12] by exploiting a TP composed of several repeated parts, which are rotated by a specific phase pattern before being transmitted. Unfortunately, the resulting schemes are not computationally efficient as they require a grid-search over the uncertainty frequency interval. The same problem occurs in [13] and [14], where no closed-form solution is provided to get the CFO estimate. A low-complexity scheme is presented in [15] to jointly compensate for the CFO and I/Q imbalances without resorting to any grid-search procedure.

The main drawback of the aforementioned methods is that they rely on specific TPs that cannot be found in any OFDM communication standard. Alternative schemes employing the IEEE 802.11a conventional repeated TP can be found

Manuscript received March 2, 2017; revised July 5, 2017 and September 26, 2017; accepted September 29, 2017. The associate editor coordinating the review of this paper and approving it for publication was J. M. Romero-Jerez. *(Corresponding author: Marco Moretti.)*

The authors are with the Dipartimento di Ingegneria dell'Informazione, University of Pisa, 56126 Pisa, Italy (e-mail: marco.moretti@iet.unipi.it).

Color versions of one or more of the figures in this paper are available online at http://ieeexplore.ieee.org.

Digital Object Identifier 10.1109/TWC.2017.2760824

in [16]–[20]. In particular, novel sine- and cosine-based estimators are derived in [16] by means of a suitable matrix formulation of the received signal samples, while a linear least squares estimation of the unsigned CFO is formulated in [18] using a general relationship among three adjacent TP segments. In [19] and [20], the useful signal component and its mirror image are interpreted as two independent sinusoidal signals, which are separated by resorting to either the ESPRIT (estimation of signal parameters via rotational invariance technique [21]) or the SAGE (space-alternating generalized expectation-maximization [22]) algorithms, respectively. In [23] the authors show that, at low and medium signal-to-noise ratio (SNR) values, the classical maximum likelihood (CML) frequency estimator, derived in [24] for a perfectly balanced receiver, performs satisfactorily even in the presence of some I/Q imbalance. Furthermore, in many situations CML exhibits improved accuracy with respect to the joint maximum likelihood (JML) estimator of the CFO, the channel distorted TP and its mirror image, which was originally presented in [11]. The reason is that JML, when applied to a repetitive TP, is subject to the sign ambiguity problem and provides poor results in the presence of small CFO values. A novel frequency estimator is also derived in [23] by exploiting some side-information about the signal-to-image ratio. This scheme, which is named constrained JML (CJML), can achieve improved accuracy with respect to CML and JML at the price of a substantial increase of the computational burden. Finally, a low-complexity scheme for the joint estimation of the CFO, channel impulse response (CIR) and I/Q imbalance is presented in [25] using the long training sequence embedded in the 802.11a preamble.

In this work, we consider an OFDM direct-conversion receiver affected by frequency-selective I/Q imbalances and further investigate the CFO recovery task using a repeated TP. In order to remove the sign ambiguity problem that affects the JML, the joint estimation of the CFO and channel impulse responses for the signal component and its mirror image is accomplished by suitably exploiting knowledge of the pilot symbols embedded in the received TP. Unfortunately, the exact ML solution cannot be implemented in practice due to its prohibitive processing requirements. Therefore, we look for simpler solutions that can be executed with affordable complexity. One of them is an approximation of the true ML estimator, which is obtained by neglecting the phase rotation induced by the residual CFO within each TP segment. The resulting scheme allows a substantial reduction of the system complexity without incurring any significant penalty in estimation accuracy with respect to the ML estimator. We also derive an alternative method based on the best linear unbiased estimation (BLUE) principle, which further reduces the processing requirements by computing the CFO estimate in closed-form. Numerical simulations indicate that the proposed schemes perform satisfactorily even in the presence of severe I/Q imbalances and outperform other existing methods. Their performance is close to the Cramer-Rao bound (CRB) provided that the order of the *overall* propagation channel (comprising the transmit and receive filters) does not exceed half the number of the pilot symbols of the TP.

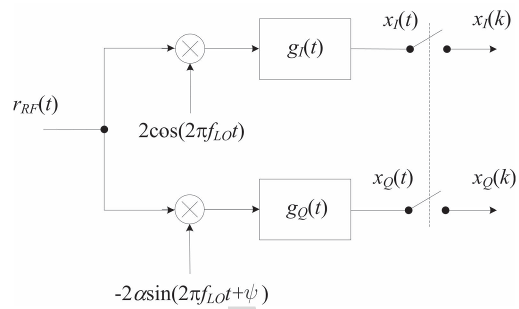

Fig. 1. Basic DCR architecture.

When such a condition is not met, the estimation accuracy decreases, especially at high SNR values.

The rest of the paper is organized as follows. Next section describes the DCR architecture and introduces the mathematical model of the received TP. In Sect. III we discuss the joint ML estimation of the CFO and channel impulse responses for the useful signal and its mirror image. Some practical adjustments are also suggested to reduce the processing load of the ML scheme. In Sect. IV we adopt the BLUE concept to get the CFO estimate in closed-form, while in Sect. V we present the CRB analysis for the considered estimation problem. Simulation results are presented in Sect. VI and, finally, some conclusions are offered in Sect. VII.

Notation: Matrices and vectors are denoted by boldface letters, with $\mathbf{I}_N$ and $\mathbf{1}_N$ being the identity matrix of order N and the N-dimensional vector with unit entries, respectively. $\mathbf{A} = \mathrm{diag}\{a(n)\,;\ n = 1, 2, \ldots, N\}$ denotes an $N \times N$ diagonal matrix with entries $a(n)$ along its main diagonal, $[\mathbf{C}]_{k,\ell}$ is the (k, ℓ)th entry of $\mathbf{C}$ and $\mathbf{B}^{-1}$ is the inverse of a matrix $\mathbf{B}$. The notation $\|\cdot\|$ represents the Euclidean norm of the enclosed vector while $\Re\mathrm{e}\{x\}$, $\Im\mathrm{m}\{x\}$, $|x|$ and $\arg\{x\}$ stand for the real and imaginary parts, the modulus, and the principal argument of a complex number x. The symbol $\otimes$ is adopted for either the convolution between continuous-time signals or the Kronecker product between matrices and/or vectors. We use $\mathrm{E}\{\cdot\}$, $(\cdot)^*$, $(\cdot)^T$ and $(\cdot)^H$ for expectation, complex conjugation, transposition and Hermitian transposition, respectively. Finally, $\tilde{\lambda}$ denotes a trial value of the unknown parameter λ.

II. System Model in the Presence of CFO and I/Q Imbalance

A. DCR Architecture

Fig. 1 illustrates the basic structure of a DCR front-end. Here, the received RF waveform $r_{RF}(t)$ is down-converted to baseband using LO signals characterized by an amplitude mismatch α and a phase error ψ. The demodulated signals are then fed to I/Q low-pass filters with different impulse responses $g_I(t)$ and $g_Q(t)$. While LO imperfections give rise to frequency-independent I/Q imbalances, filter mismatches vary over the signal bandwidth, thereby resulting into a frequency-selective imbalance [11]. We call $r(t)$ the complex envelope of $r_{RF}(t)$ with respect to the carrier frequency f_0, and let $\Delta f = f_0 - f_{LO}$ be the offset between the carrier and LO frequencies. Hence, we can write the received waveform as $r_{RF}(t) = \Re\text{e}\{r(t)e^{j2\pi(f_{LO}+\Delta f)t}\}$, with

$$r(t) = s(t) \otimes \upsilon(t) + n(t). \tag{1}$$

In the above equation, $s(t)$ and $\upsilon(t)$ are the baseband representations of the transmitted signal and propagation channel, respectively, while $n(t)$ is circularly symmetric AWGN with two-sided power spectral density $2N_0$. As shown in Fig. 1, we denote by $x(t) = x_I(t) + jx_Q(t)$ the complex down-converted signal at the output of the mismatched I/Q filters. Then, after standard manipulations we get

$$x(t) = e^{j2\pi\Delta ft}[s(t) \otimes h(t)] + e^{-j2\pi\Delta ft}[s^*(t) \otimes q(t)] + w(t) \tag{2}$$

where the first term is the direct signal component, the second term represents self-image interference, and $w(t)$ accounts for the noise contribution. The equivalent CIRs $h(t)$ and $q(t)$ appearing in (2) are expressed by [11]

$$\begin{aligned} h(t) &= \upsilon(t) \otimes p_+(t)e^{-j2\pi\Delta ft} \\ q(t) &= \upsilon^*(t) \otimes p_-(t)e^{j2\pi\Delta ft} \end{aligned} \tag{3}$$

with

$$\begin{aligned} p_+(t) &= \frac{1}{2}[g_I(t) + \alpha g_Q(t)e^{-j\psi}] \\ p_-(t) &= \frac{1}{2}[g_I(t) - \alpha g_Q(t)e^{j\psi}] \end{aligned} \tag{4}$$

while the noise term $w(t) = w_I(t) + jw_Q(t)$ takes the form

$$w(t) = n(t)e^{j2\pi\Delta ft} \otimes p_+(t) + n^*(t)e^{-j2\pi\Delta ft} \otimes p_-(t). \tag{5}$$

Substituting (4) into (5), it is found that $w_I(t)$ and $w_Q(t)$ are zero-mean Gaussian processes with auto- and cross-correlation functions

$$\begin{aligned} \mathrm{E}\{w_I(t)w_I(t+\tau)\} &= N_0[g_I(\tau) \otimes g_I(-\tau)] \\ \mathrm{E}\{w_Q(t)w_Q(t+\tau)\} &= \alpha^2 N_0[g_Q(\tau) \otimes g_Q(-\tau)] \\ \mathrm{E}\{w_I(t)w_Q(t+\tau)\} &= -\alpha N_0 \sin\psi[g_I(\tau) \otimes g_Q(-\tau)]. \end{aligned} \tag{6}$$

Since the real and imaginary components of $w(t)$ are generally cross-correlated with different auto-correlation functions, we conclude that, in general, the noise process at the ouptut of a DCR front-end is not circularly symmetric.

B. Mathematical Model of the Received TP

We consider an OFDM burst-mode communication system, where each burst is preceded by a TP to assist the synchronization and channel estimation functions. In contrast to many related works, where the TP is suitably designed to cope with I/Q imbalances [6]–[15], in this study we assume a conventional periodic preamble composed by $M_T \geq 2$ repeated segments. Each segment contains P time-domain samples, which are obtained as the inverse discrete Fourier transform (IDFT) of P pilot symbols $\{c(n); n = 0, 1, \ldots, P-1\}$. Such a preamble is general enough to include both the short training sequence ($M_T = 10$, $P = 16$) and the long training sequence ($M_T = 2$, $P = 64$) of the 802.11a WLAN standard [1]. In the former case, a number $M_G \geq 1$ of segments serve as a cyclic prefix (CP) to avoid interblock interference, while the remaining $M = M_T - M_G$ segments are exploited for synchronization purposes. In the latter case we have $M_G = 0$ since the long training sequence is preceded by its own CP.

For simplicity, we consider a discrete-time baseband signal model with signaling interval T_s. The TP samples are thus given by

$$s[l] = \frac{1}{\sqrt{P}} \sum_{n=0}^{P-1} c(n)e^{j2\pi nl/P} \quad -N_G \leq l \leq MP-1 \tag{7}$$

where N_G is the CP duration normalized by T_s. After propagating through the multipath channel, the received signal $x[l] = x(lT_s)$ is plagued by CFO and frequency-selective I/Q imbalances. Bearing in mind (2) and assuming that $h(t)$ and $q(t)$ have support $[0, LT_s)$ with $L \leq N_G$, we have

$$\begin{aligned} x[l] = {} & \frac{e^{jl\phi}}{\sqrt{P}} \sum_{k=0}^{L-1} h[k] \sum_{n=0}^{P-1} c(n)e^{j2\pi n(l-k)/P} \\ & + \frac{e^{-jl\phi}}{\sqrt{P}} \sum_{k=0}^{L-1} q[k] \sum_{n=0}^{P-1} c^*(n)e^{-j2\pi n(l-k)/P} + w[l] \end{aligned} \tag{8}$$

for $0 \leq l \leq MP-1$. In the above equation, $h[k]$ and $q[k]$ is the shorthand notation for $h(kT_s)$ and $q(kT_s)$, respectively, $w[l]$ is the noise sample and we have defined

$$\phi = 2\pi\Delta fT_s. \tag{9}$$

To proceed further, we arrange the quantities $x[l]$ into an $MP-$ dimensional vector $\mathbf{x} = (x[0], x[1], \ldots, x[MP-1])^T$ and let $\mathbf{C} = \text{diag}\{c(n), n = 0, 1, \ldots, P-1\}$. Then, we can put (8) in matrix notation as

$$\mathbf{x} = \boldsymbol{\Gamma}(\phi)\mathbf{G}_1\mathbf{C}\mathbf{G}_2\mathbf{h} + \boldsymbol{\Gamma}(-\phi)\mathbf{G}_1^*\mathbf{C}^*\mathbf{G}_2^*\mathbf{q} + \mathbf{w} \tag{10}$$

where $\mathbf{h} = (h[0], h[1], \ldots, h[L-1])^T$ and $\mathbf{q} = (q[0], q[1], \ldots, q[L-1])^T$ are the $L-$dimensional CIR vectors, $\mathbf{w} = (w[0], w[1], \ldots, w[MP-1])^T$ represents the noise contribution and $\boldsymbol{\Gamma}(\phi) = \text{diag}\{e^{jl\phi}, l = 0, 1, \ldots, MP-1\}$. Finally, $\mathbf{G}_2$ is a $(P \times L)-$dimensional matrix with entries

$$[\mathbf{G}_2]_{n,k} = e^{-j2\pi(n-1)(k-1)/P} \quad n = 1, 2, \ldots, P \;\; k = 1, 2, \ldots, L \tag{11}$$

while $\mathbf{G}_1$ has dimension $MP \times P$ and can be expressed as

$$\mathbf{G}_1 = \mathbf{1}_M \otimes \mathbf{F}_P \tag{12}$$

where $\mathbf{F}_P$ is the unitary $P-$point IDFT matrix with entries

$$[\mathbf{F}_P]_{n,k} = \frac{1}{\sqrt{P}} e^{j2\pi(n-1)(k-1)/P} \quad n, k = 1, 2, \ldots, P. \tag{13}$$

III. Joint ML Estimation of the CFO and CIR Vectors

A. Estimator Design

Inspection of (3) and (4) indicates that the equivalent CIRs $h(t)$ and $q(t)$ are mathematically related to the LO imbalance parameters α and ψ, the CFO Δf and the propagation channel $\upsilon(t)$. All these quantities can in principle be recovered from the observation vector $\mathbf{x}$ by resorting to some optimality criterion. Albeit effective, this approach would result into a prohibitively complex estimation process, where an exhaustive grid-search has to be employed to localize the optimum point of a multidimensional cost function. For this reason, we follow a more pragmatic strategy, which ignores the dependence of $\mathbf{u} = [\mathbf{h}^T \ \ \mathbf{q}^T]^T$ on the other unknown parameters and looks for the joint ML estimates of ($\mathbf{u}$, ϕ). Despite the remarkable advantage in terms of system complexity, the joint recovery of ($\mathbf{u}$, ϕ) is still complicated by the fact that the likelihood function does not take the classical form of a multivariate Gaussian probability density function due to the structure of the noise vector $\mathbf{w}$, which is not circularly symmetric. To overcome such a difficulty, for the time being we assume that $\mathbf{w}$ is a zero-mean circularly symmetric Gaussian (ZMCSG) complex vector with covariance matrix $\sigma_w^2 \mathbf{I}_{MP}$. Although this assumption holds true only in a perfectly balanced DCR architecture, it has been used even in the presence of non-negligible I/Q imbalances to derive novel frequency recovery schemes [26]. We point out that in our study the white noise assumption is adopted only to derive the CFO estimators and to analytically compute their accuracy, while the true noise statistics shown in (6) are employed in the numerical analysis to assess the system performance in a realistic scenario.

We start our analysis by rewriting (10) in a more compact form as

$$\mathbf{x} = \mathbf{A}(\phi)\mathbf{u} + \mathbf{w} \tag{14}$$

where the $(MP \times 2L)$−dimensional matrix $\mathbf{A}(\phi)$ is expressed by

$$\mathbf{A}(\phi) = [\boldsymbol{\Gamma}(\phi)\mathbf{G}_1\mathbf{C}\mathbf{G}_2 \ \ \boldsymbol{\Gamma}(-\phi)\mathbf{G}_1^*\mathbf{C}^*\mathbf{G}_2^*]. \tag{15}$$

Applying the ML estimation principle to the observation vector $\mathbf{x}$ under the ZMCSG assumption for $\mathbf{w}$, leads to the following maximization problem

$$\{\hat{\mathbf{u}}, \hat{\phi}\} = \arg\max_{\{\tilde{\mathbf{u}}, \tilde{\phi}\}} \left\{ -\left\| \mathbf{x} - \mathbf{A}(\tilde{\phi})\tilde{\mathbf{u}} \right\|^2 \right\}. \tag{16}$$

For a fixed value of $\tilde{\phi}$, the maximum is achieved at

$$\hat{\mathbf{u}}(\tilde{\phi}) = \left[\mathbf{A}^H(\tilde{\phi})\mathbf{A}(\tilde{\phi}) \right]^{-1} \mathbf{A}^H(\tilde{\phi})\mathbf{x} \tag{17}$$

which, after substitution into (16), yields the CFO metric in the form

$$\Lambda\ (\tilde{\phi}) = \mathbf{x}^H \mathbf{A}(\tilde{\phi}) \left[\mathbf{A}^H(\tilde{\phi})\mathbf{A}(\tilde{\phi}) \right]^{-1} \mathbf{A}^H(\tilde{\phi})\mathbf{x}. \tag{18}$$

It is worth noting that letting $L = P$ and replacing $\mathbf{G}_1\mathbf{C}\mathbf{G}_2$ in (15) with $\mathbf{1}_M \otimes \mathbf{I}_P$ leads to the JML estimator originally presented in [11], which was later applied to a repeated preamble in [23]. Compared to JML, the metric (18) exploits the mathematical structure of the received TP specified by the matrix $\mathbf{A}(\phi)$, which depends on the pilot symbols $\{c(n)\}$ and the DFT/IDFT matrices $\mathbf{G}_1$ and $\mathbf{G}_2$ as shown in (15). Accordingly, in the sequel the CFO estimator maximizing the metric (18) is referred to as the structured JML (SJML), i.e.

$$\hat{\phi}_{SJML} = \arg\max_{\tilde{\phi}} \{\Lambda(\tilde{\phi})\}. \tag{19}$$

TABLE I

COMPLEXITY OF THE INVESTIGATED SCHEMES

Algorithm	Number of flops	WLAN scenario
SJML	$16LMPN_\phi$	$1,572,864$
RC-SJML	$2LM(4P+2M-3)+5N_\phi \log_2 N_\phi$	$11,872$
BLUE	$LM(8P+3M-4)+M/2$	$7,108$
CML	$(4MP-3)(M-1)+5N_\phi \log_2 N_\phi$	$8,043$
JML	$8P(2M+1)N_\phi$	$278,528$
RCE	$4(2MP+1)L$	$6,168$

In order to assess the complexity of SJML, it is convenient to put (18) into the equivalent form

$$\Lambda\ (\tilde{\phi}) = \left\| \mathbf{L}_c^H(\tilde{\phi})\mathbf{A}^H(\tilde{\phi})\mathbf{x} \right\|^2 \tag{20}$$

where $\mathbf{L}_c(\tilde{\phi})\mathbf{L}_c^H(\tilde{\phi})$ is the Cholesky factorization of $\left[\mathbf{A}^H(\tilde{\phi})\mathbf{A}(\tilde{\phi})\right]^{-1}$. Then, we see that evaluating $\Lambda\ (\tilde{\phi})$ approximately needs $2LMP$ complex multiplications plus $2LMP$ complex additions for each value of $\tilde{\phi}$, which corresponds to $16LMP$ floating point operations (flops). In writing these figures we have borne in mind that a complex multiplication amounts to four real multiplications plus two real additions, while a complex additions is equivalent to two real additions. Furthermore, we have assumed that matrices $\mathbf{L}_c^H(\tilde{\phi})\mathbf{A}^H(\tilde{\phi})$ are pre-computed and stored in the receiver. The overall computational requirement of SJML is summarized in the first row of Table I, where we have denoted by N_ϕ the number of candidate values $\tilde{\phi}$. Since in the presence of a considerable CFO uncertainty the number N_ϕ can be quite large, we expect that SJML cannot be implemented with affordable complexity. This justifies the search for alternative schemes with less computational requirements and good estimation accuracy.

B. Reduced-Complexity CFO Estimation

We begin by partitioning vector $\mathbf{x}$ into M subvectors $\{\mathbf{x}_m; m = 0, 1, \ldots, M-1\}$, where $\mathbf{x}_m$ collects the P samples belonging to the mth received TP segment. Then, letting $\mathbf{x} = [\mathbf{x}_0^T \ \ \mathbf{x}_1^T \ \cdots \ \mathbf{x}_{M-1}^T]^T$ and bearing in mind (10) and (12), the mathematical model of $\mathbf{x}_m$ is found to be

$$\mathbf{x}_m = e^{jmP\phi}\boldsymbol{\Gamma}_P(\phi)\mathbf{F}_P\mathbf{C}\mathbf{G}_2\mathbf{h} + e^{-jmP\phi}\boldsymbol{\Gamma}_P(-\phi)\mathbf{F}_P^*\mathbf{C}^*\mathbf{G}_2^*\mathbf{q} + \mathbf{w}_m \tag{21}$$

where $\mathbf{w}_m$ is the mth subvector of $\mathbf{w} = [\mathbf{w}_0^T \ \ \mathbf{w}_1^T \ \cdots \ \mathbf{w}_{M-1}^T]^T$ and $\boldsymbol{\Gamma}_P(\phi) = \mathrm{diag}\{e^{jl\phi},\ l = 0, 1, \ldots, P-1\}$. In order to simplify the SJML metric, we make the following approximation

$$\boldsymbol{\Gamma}_P(\phi) \simeq e^{j(P-1)\phi/2}\mathbf{I}_P \tag{22}$$

which amounts to replacing the linearly increasing phase shift $l\phi$ for $l = 0, 1, \ldots, P-1$ by its average value $(P-1)\phi/2$. Denoting by $|\phi|^{(\max)}$ the largest value of $|\phi|$, the maximum phase deviation between the entries of $\boldsymbol{\Gamma}_P(\phi)$ and $e^{j(P-1)\phi/2}\mathbf{I}_P$ turns out to be $(P-1)\,|\phi|^{(\max)}/2$. This suggests that approximation (22) becomes more and more questionable as P increases, and limits the range of P as discussed later in Sect. VI B.

Plugging (22) into (21) yields

$$\mathbf{x}_m \simeq e^{j(2mP+P-1)\phi/2}\mathbf{F}_P\mathbf{C}\mathbf{G}_2\mathbf{h} + e^{-j(2mP+P-1)\phi/2}\mathbf{F}_P^*\mathbf{C}^*\mathbf{G}_2^*\mathbf{q} + \mathbf{w}_m \quad (23)$$

which can also be rewritten in a more compact form as

$$\mathbf{x}_m = \mathbf{T}\mathbf{u}_m + \mathbf{w}_m \quad (24)$$

where $\mathbf{u}_m$ is a $2L-$dimensional vector expressed by

$$\mathbf{u}_m = \begin{bmatrix} e^{j(2mP+P-1)\phi/2}\mathbf{h} \\ e^{-j(2mP+P-1)\phi/2}\mathbf{q} \end{bmatrix} \quad (25)$$

and $\mathbf{T}$ is the following matrix of dimension $P \times (2L)$

$$\mathbf{T} = \begin{bmatrix}\mathbf{T}_1 \ \mathbf{T}_1^*\end{bmatrix} \quad (26)$$

with $\mathbf{T}_1 = \mathbf{F}_P\mathbf{C}\mathbf{G}_2$. From the simplified model (24), the ML estimate of $\mathbf{u}_m$ is computed as

$$\hat{\mathbf{u}}_m = (\mathbf{T}^H\mathbf{T})^{-1}\mathbf{T}^H\mathbf{x}_m. \quad (27)$$

Then, recalling the structure of $\mathbf{u}_m$ shown in (25), we observe that the first L elements of $\hat{\mathbf{u}}_m$ provide an estimate of $e^{j(2mP+P-1)\phi/2}\mathbf{h}$, while the last L elements provide an estimate of $e^{-j(2mP+P-1)\phi/2}\mathbf{q}$. Since in a practical scenario the energy of $\mathbf{q}$ is typically much smaller than the energy of $\mathbf{h}$, in the sequel we only exploit the first part of $\hat{\mathbf{u}}_m$ ($m = 0, 1, \ldots, M-1$) to retrieve the CFO. This approach has the remarkable advantage of reducing the system complexity without leading to any significant loss in estimation accuracy. Hence, substituting (24) into (27) and denoting by $\boldsymbol{\xi}_m$ the first L entries of $\hat{\mathbf{u}}_m$, we get

$$\boldsymbol{\xi}_m = e^{j(2mP+P-1)\phi/2}\mathbf{h} + \boldsymbol{\eta}_m \quad (28)$$

where $\boldsymbol{\eta}_m$ is a zero-mean Gaussian vector with covariance matrix $\mathbf{C}_\eta = \sigma_w^2\mathbf{K}$, and $\mathbf{K}$ is an $L-$dimensional matrix with entries $[\mathbf{K}]_{i,j} = [(\mathbf{T}^H\mathbf{T})^{-1}]_{i,j}$ for $1 \le i, j \le L$. Observing that

$$\mathbf{T}^H\mathbf{T} = \begin{bmatrix} \mathbf{T}_1^H\mathbf{T}_1 & \mathbf{T}_1^H\mathbf{T}_1^* \\ \mathbf{T}_1^T\mathbf{T}_1 & \mathbf{T}_1^T\mathbf{T}_1^* \end{bmatrix} \quad (29)$$

from the inversion formula of a partitioned matrix we have [27, p. 572]

$$\mathbf{K} = [\mathbf{T}_1^H\mathbf{T}_1 - \mathbf{T}_1^H\mathbf{T}_1^*(\mathbf{T}_1^T\mathbf{T}_1^*)^{-1}\mathbf{T}_1^T\mathbf{T}_1]^{-1}. \quad (30)$$

We now derive the joint ML estimate of the unknown parameters $(\mathbf{h},\phi)$ starting from the observation vectors $\{\boldsymbol{\xi}_m; m = 0, 1, \ldots, M-1\}$. Neglecting irrelevant terms independent of $(\tilde{\mathbf{h}}, \tilde{\phi})$, we may write the log-likelihood function (LLF) in the form

$$\Psi\,(\tilde{\mathbf{h}}, \tilde{\phi}) = 2\Re\mathrm{e}\left\{\tilde{\mathbf{h}}^H\mathbf{K}^{-1}\sum_{m=0}^{M-1} e^{-j(2mP+P-1)\tilde{\phi}/2}\boldsymbol{\xi}_m\right\} - M(\tilde{\mathbf{h}}^H\mathbf{K}^{-1}\tilde{\mathbf{h}}). \quad (31)$$

Maximizing $\Psi\,(\tilde{\mathbf{h}}, \tilde{\phi})$ with respect to $\tilde{\mathbf{h}}$ yields

$$\hat{\mathbf{h}}(\tilde{\phi}) = \frac{1}{M}\sum_{m=0}^{M-1} e^{-j(2mP+P-1)\tilde{\phi}/2}\boldsymbol{\xi}_m \quad (32)$$

and plugging this result into (31) produces the concentrated likelihood function for the estimation of ϕ as

$$\Psi_c(\tilde{\phi}) = \left\| \sum_{m=0}^{M-1} e^{-jmP\tilde{\phi}}\mathbf{y}_m \right\|^2 \quad (33)$$

with $\mathbf{y}_m = \mathbf{K}^{-1/2}\boldsymbol{\xi}_m$. After some standard manipulations, we can put $\Psi_c(\tilde{\phi})$ in the equivalent form

$$\Psi_c(\tilde{\phi}) = \sum_{m=1}^{M-1} \Re\mathrm{e}\left\{R(m)e^{-jmP\tilde{\phi}}\right\} \quad (34)$$

where the quantities $\{R(m)\}$ are defined as

$$R(m) = \sum_{k=m}^{M-1} \mathbf{y}_{k-m}^H\mathbf{y}_k \quad 1 \le m \le M-1. \quad (35)$$

In the sequel, the CFO estimator maximizing $\Psi_c(\tilde{\phi})$ is referred to as the reduced-complexity SJML (RC-SJML), i.e.

$$\hat{\phi}_{RC-SJML} = \arg\max_{\tilde{\phi}}\{\Psi_c(\tilde{\phi})\}. \quad (36)$$

C. Remarks

1) Inspection of (34) reveals that $\Psi_c(\tilde{\phi})$ is periodic of period $2\pi/P$, meaning that the estimator provides ambiguous estimates unless ϕ is confined within the interval $|\phi| \le \pi/P$. Recalling the relationship (9) between ϕ and Δf, it turns out that the estimation range of RC-SJML is given by $|\Delta f| \le 1/(2PT_s)$.

2) The maximum of $\Psi_c(\tilde{\phi})$ can be found through the following two-step procedure. In the first step (coarse search), the CFO metric is evaluated over a set of $\tilde{\phi}$ values, say $\left\{\tilde{\phi}_n\right\}$, covering the uncertainty range of ϕ and the location $\tilde{\phi}_M$ of the maximum is determined over this set. In the second step (fine search), the quantities $\{\Psi_c(\tilde{\phi}_n)\}$ are interpolated to locate the local maximum nearest to $\tilde{\phi}_M$. The coarse search can be efficiently performed using Fast Fourier Transform (FFT) techniques. Specifically, we consider the following zero-padded sequence of length $N_\phi = M\gamma_{pr}$

$$R_{ZP}(m) = \begin{cases} R(m) & 1 \le m \le M-1 \\ 0 & M \le m \le N_\phi - 1 \ \text{ and } m = 0 \end{cases} \quad (37)$$

where $\gamma_{pr} \ge 1$ is an integer design parameter called *pruning factor*. Then, we compute the N_ϕ-point ($-N_\phi/2 < n \le N_\phi/2$) FFT of $R_{ZP}(m)$

$$\mathrm{FFT}\{R_{ZP}(m)\} = \sum_{m=0}^{N_\phi-1} R_{ZP}(m)e^{-j2\pi mn/N_\phi} \quad (38)$$

and observe that the real part of the FFT provides samples of the metric $\Psi_c(\tilde{\phi})$ evaluated at

$$\tilde{\phi}_n = \frac{2\pi n}{PM\gamma_{pr}}, \quad -N_\phi/2 < n \le N_\phi/2. \quad (39)$$

The maximum of the set $\{\Psi_c(\tilde{\phi}_n)\}$ is eventually sought, and this provides the coarse estimate of ϕ. From (39), it is seen that the pruning factor determines the granularity of the coarse search.

3) In assessing the complexity of RC-SJML, we observe that evaluating vectors $\mathbf{y}_m$ for $0 \leq m \leq M-1$ needs $8LMP - 2LM$ flops, while nearly $4LM(M-1)$ flops are required to obtain the correlations $R(m)$ for $1 \leq m \leq M-1$ starting from $\mathbf{y}_m$. Finally, the FFT of the sequence $R_{ZP}(m)$ is computed with $(N_\phi/2)\log_2(N_\phi)$ complex multiplications plus $N_\phi \log_2(N_\phi)$ complex additions, which corresponds to additional $5N_\phi \log_2(N_\phi)$ flops. The overall operations are summarized in the second row of Table I.

4) Evaluating $\hat{\mathbf{u}}_m$ as shown in (27) requires the invertibility of the $(2L)-$dimensional matrix $\mathbf{T}^H\mathbf{T}$, which is attainable only if $\mathbf{T}$ has full-rank $2L$. From (26), we see that rank($\mathbf{T}$) depends on $\mathbf{T}_1 = \mathbf{F}_P\mathbf{C}\mathbf{G}_2$ and, ultimately, on the structure of $\mathbf{C}$. In particular, when considering the short training sequence (STS) of the 802.11a preamble we have rank($\mathbf{T}$) $=\min\ (2L, N_p)$, where $N_p = 12$ is the number of non-zero pilot symbols $\{c(n)\}$. In such a case, application of RC-SJML requires that $L \leq N_p/2$, which poses a limit to the maximum channel order that can be handled. When such a constraint is not fulfilled, the problem arises as how to compute vector $\hat{\mathbf{u}}_m$. One possibility is to replace $(\mathbf{T}^H\mathbf{T})^{-1}$ in (27) by $(\mathbf{T}^H\mathbf{T}+\lambda\mathbf{I}_{2L})^{-1}$, where $\lambda > 0$ is a regularization parameter which ensures the invertibility of $\mathbf{T}^H\mathbf{T}+\lambda\mathbf{I}_{2L}$. A good choice for such a parameter is $\lambda = \sigma_w^2$, as in this case $\hat{\mathbf{u}}_m$ reduces to the minimum mean square error (MMSE) estimate of $\mathbf{u}_m$ based on the observation vector $\mathbf{x}_m$. Alternatively, we can replace the true channel order L by $\overline{L} = N_p/2$ for the sole purpose of evaluting $\hat{\mathbf{u}}_m$, and let the RC-SJML operate in a mismatched mode. In such a case, the estimation accuracy is expected to worsen more and more as the difference $L - \overline{L}$ grows large. This intuition will be checked later through numerical measurements.

IV. CFO Estimation in Closed-Form

Although RC-SJML can provide a remarkable reduction of the processing requirements with respect to SJML, the maximization problem in (36) still requires a search over the uncertainty range of ϕ, which may be cumbersome in certain applications. To overcome this problem, we introduce an alternative scheme that is able to estimate the CFO in closed-form. Our approach is based on some heuristic reasoning and exploits the correlations $\{R(m);\ 1 \leq m \leq M-1\}$ defined in (35).

We begin by deriving the mathematical model of vectors $\mathbf{y}_m = \mathbf{K}^{-1/2}\boldsymbol{\xi}_m$, with $\boldsymbol{\xi}_m$ as shown in (28). Letting

$$\mathbf{h}_{eq} = \mathbf{K}^{-1/2}\mathbf{h} \tag{40}$$

we get

$$\mathbf{y}_m = e^{j(2mP+P-1)\phi/2}(\mathbf{h}_{eq}+\mathbf{n}_m) \tag{41}$$

where $\mathbf{n}_m = \mathbf{K}^{-1/2}\boldsymbol{\eta}_m e^{-j(2mP+P-1)\phi/2}$ is a zero-mean Gaussian vector with covariance matrix $\mathbf{C}_n = \sigma_w^2\mathbf{I}_L$. Substituting this result into (35) produces

$$R(m) = (M-m)\left\|\mathbf{h}_{eq}\right\|^2 e^{jmP\phi}[1+\gamma(m)] \quad 1 \leq m \leq M-1 \tag{42}$$

with

$$\gamma\ (m) = \frac{1}{(M-m)\left\|\mathbf{h}_{eq}\right\|^2}\sum_{k=m}^{M-1}[\mathbf{h}_{eq}^H\mathbf{n}_k+\mathbf{n}_{k-m}^H\mathbf{h}_{eq}+\mathbf{n}_{k-m}^H\mathbf{n}_k]. \tag{43}$$

Inspection of (42) reveals that the unknown parameter ϕ is linearly related to the argument of $R(m)$. Hence, we define the angles

$$\theta(m) = \arg\{R(m)R^*(m-1)\} \quad 1 \leq m \leq H \tag{44}$$

where H is a design parameter not greater than $M-1$ and $R(0)$ is arbitrarily set to unity. Furthermore, we assume large SNR values such that $\arg\{1+\gamma(m)\} \simeq \gamma_I(m)$, with $\gamma_I(m)$ being the imaginary part of $\gamma(m)$. In these circumstances, from (42) we have

$$\theta(m) \simeq [P\phi + \gamma_I(m) - \gamma_I(m-1)]_{2\pi} \tag{45}$$

where $[x]_{2\pi}$ denotes the value of x reduced to the interval $[-\pi, \pi)$. If ϕ is adequately smaller than π/P, the quantity in brackets in (45) is (with high probability) less than π and $\theta(m)$ reduces to

$$\theta(m) = P\phi + \eta(m) \tag{46}$$

with $\eta\ (m) = \gamma_I(m) - \gamma_I(m-1)$. It is worth noting that the linear model (46) is exactly the same presented in [28] in the context of CFO recovery for OFDM receiver without any I/Q imbalance. The BLUE of ϕ as a function of the observation variables $\boldsymbol{\theta} = [\theta\ (1), \theta\ (2), \ldots, \theta\ (H)]^T$ is given by [27]

$$\hat{\phi}_{BLUE} = \frac{1}{P}\sum_{m=1}^{H}\alpha_{BLUE}(m)\theta(m) \tag{47}$$

where $\alpha_{BLUE}(m)$ is the mth element of

$$\boldsymbol{\alpha}_{BLUE} = \frac{\mathbf{C}_\eta^{-1}\mathbf{1}}{\mathbf{1}^T\mathbf{C}_\eta^{-1}\mathbf{1}} \tag{48}$$

and $\mathbf{C}_\eta$ is the covariance matrix of $\boldsymbol{\eta} = [\eta(1), \eta(2), \ldots, \eta(H)]^T$. The variance of $\hat{\phi}_{BLUE}$ is expressed by

$$\mathrm{var}(\hat{\phi}_{BLUE}) = \frac{1}{P^2}\frac{1}{\mathbf{1}^T\mathbf{C}_\eta^{-1}\mathbf{1}} \tag{49}$$

and depends on the design parameter H. In [28] it is shown that the minimum of var($\hat{\phi}_{BLUE}$) is achieved when $H = M/2$. In such a case we have

$$\alpha_{BLUE}(m) = 3\frac{4(M-m)(M-m+1)-M^2}{2M(M^2-1)} \tag{50}$$

and

$$\mathrm{var}(\hat{\phi}_{BLUE}) = \frac{6\sigma_w^2}{MP^2(M^2-1)\left\|\mathbf{h}_{eq}\right\|^2}. \tag{51}$$

The complexity of BLUE is assessed by observing that, besides the $8LMP - 2LM$ flops required to get vectors $\mathbf{y}_m$ for $0 \leq m \leq M-1$, additional $LM(3M-2) - M$ flops are involved in the evaluation of $R(m)$ for $1 \leq m \leq M/2$. The estimate $\hat{\phi}_{BLUE}$ is eventually obtained from the correlations $R(m)$ with $3M/2$ flops. This leads to the overall complexity listed in the third row of Table I.

$$\dot{\mathbf{B}}(\phi) = \begin{bmatrix} \mathbf{M} & \mathbf{0} \\ \mathbf{0} & \mathbf{M} \end{bmatrix} \begin{bmatrix} -\Im\mathrm{m}\{\mathbf{A}_1(\phi)\} & -\Re\mathrm{e}\{\mathbf{A}_1(\phi)\} & -\Im\mathrm{m}\{\mathbf{A}_1(\phi)\} & \Re\mathrm{e}\{\mathbf{A}_1(\phi)\} \\ \Re\mathrm{e}\{\mathbf{A}_1(\phi)\} & -\Im\mathrm{m}\{\mathbf{A}_1(\phi)\} & -\Re\mathrm{e}\{\mathbf{A}_1(\phi)\} & -\Im\mathrm{m}\{\mathbf{A}_1(\phi)\} \end{bmatrix} \tag{56}$$

V. CRB Analysis

It is interesting to compare the accuracy of the CFO estimation algorithms derived in the previous Sections with the relevant CRB. The latter is obtained starting from the signal model given in (14)-(15), and using the true noise statistics expressed in (6). We begin by arranging the received samples $\mathbf{x}$ into a real-valued vector $\check{\mathbf{x}} = [\mathbf{x}_I^T \ \mathbf{x}_Q^T]^T$, with $\mathbf{x}_I = \Re\mathrm{e}\{\mathbf{x}\}$ and $\mathbf{x}_Q = \Im\mathrm{m}\{\mathbf{x}\}$. Then, we define the real-valued CIR vector as $\check{\mathbf{u}} = [\mathbf{h}_{re}^T \ \mathbf{h}_{im}^T \ \mathbf{q}_{re}^T \ \mathbf{q}_{im}^T]^T$, where $\mathbf{h}_{re}$ and $\mathbf{q}_{re}$ are the real parts of $\mathbf{h}$ and $\mathbf{q}$, respectively, while $\mathbf{h}_{im}$ and $\mathbf{q}_{im}$ are the imaginary parts. Finally, letting $\check{\mathbf{w}} = [\mathbf{w}_I^T \ \mathbf{w}_Q^T]^T$, with $\mathbf{w}_I = \Re\mathrm{e}\{\mathbf{w}\}$ and $\mathbf{w}_Q = \Im\mathrm{m}\{\mathbf{w}\}$, we may rewrite (14) as

$$\check{\mathbf{x}} = \mathbf{B}(\phi)\check{\mathbf{u}} + \check{\mathbf{w}} \tag{52}$$

where

$$\mathbf{B}(\phi) = \begin{bmatrix} \Re\mathrm{e}\{\mathbf{A}_1(\phi)\} & -\Im\mathrm{m}\{\mathbf{A}_1(\phi)\} & \Re\mathrm{e}\{\mathbf{A}_1(\phi)\} & \Im\mathrm{m}\{\mathbf{A}_1(\phi)\} \\ \Im\mathrm{m}\{\mathbf{A}_1(\phi)\} & \Re\mathrm{e}\{\mathbf{A}_1(\phi)\} & -\Im\mathrm{m}\{\mathbf{A}_1(\phi)\} & \Re\mathrm{e}\{\mathbf{A}_1(\phi)\} \end{bmatrix} \tag{53}$$

with $\mathbf{A}_1(\phi) = \mathbf{\Gamma}(\phi)\mathbf{G}_1\mathbf{C}\mathbf{G}_2 = \mathbf{\Gamma}(\phi)\,(\mathbf{1}_M \otimes \mathbf{T}_1)$. To proceed further, we denote by $\mathbf{C}_{\check{w}}$ the covariance matrix of the Gaussian vector $\check{\mathbf{w}}$, which can be computed through (6). Then, letting the set of unknown parameters be $\boldsymbol{\chi} = (\phi, \check{\mathbf{u}})$, it is found that the Fisher information matrix $\mathbf{\Omega}$ for the estimation of $\boldsymbol{\chi}$ takes the following form [27, Sec. 3.9]

$$\mathbf{\Omega} = \begin{bmatrix} \omega_{\phi\phi} & \boldsymbol{\omega}_{\phi\check{u}}^T \\ \boldsymbol{\omega}_{\phi\check{u}} & \mathbf{\Omega}_{\check{u}\check{u}} \end{bmatrix} \tag{54}$$

where

$$\begin{aligned} \omega_{\phi\phi} &= \check{\mathbf{u}}^T\dot{\mathbf{B}}^T(\phi)\mathbf{C}_{\check{w}}^{-1}\dot{\mathbf{B}}(\phi)\check{\mathbf{u}} \\ \boldsymbol{\omega}_{\phi\check{u}} &= \mathbf{B}^T(\phi)\mathbf{C}_{\check{w}}^{-1}\dot{\mathbf{B}}(\phi)\check{\mathbf{u}} \\ \mathbf{\Omega}_{\check{u}\check{u}} &= \mathbf{B}^T(\phi)\mathbf{C}_{\check{w}}^{-1}\mathbf{B}(\phi) \end{aligned} \tag{55}$$

and we have denoted by $\dot{\mathbf{B}}(\phi)$ the derivative of $\mathbf{B}(\phi)$ with respect to ϕ. Taking (53) into account, yields (56), as shown at the top of this page, with $\mathbf{M} = \mathrm{diag}\{0, 1, \ldots, MP-1\}$. The CRB for the estimation of ϕ is the $(1,1)$th entry of $\mathbf{\Omega}^{-1}$, i.e.

$$\mathrm{CRB}(\phi) = \frac{1}{\omega_{\phi\phi} - \boldsymbol{\omega}_{\phi\check{u}}^T\mathbf{\Omega}_{\check{u}\check{u}}^{-1}\boldsymbol{\omega}_{\phi\check{u}}} \tag{57}$$

while the CRBs for the estimation of the entries of $\check{\mathbf{u}}$ are the diagonal elements of the following matrix

$$\mathbf{J} = \mathbf{\Omega}_{\check{u}\check{u}}^{-1} + \frac{\mathbf{\Omega}_{\check{u}\check{u}}^{-1}\boldsymbol{\omega}_{\phi\check{u}}\boldsymbol{\omega}_{\phi\check{u}}^T\mathbf{\Omega}_{\check{u}\check{u}}^{-1}}{\omega_{\phi\phi} - \boldsymbol{\omega}_{\phi\check{u}}^T\mathbf{\Omega}_{\check{u}\check{u}}^{-1}\boldsymbol{\omega}_{\phi\check{u}}}. \tag{58}$$

The *normalized* CRBs for the estimation of $\mathbf{h}$ and $\mathbf{q}$ are eventually given by

$$\mathrm{CRB}(\mathbf{h}) = \frac{1}{\|\mathbf{h}\|^2}\sum_{m=1}^{2L}[\mathbf{J}]_{m,m} \tag{59}$$

and

$$\mathrm{CRB}(\mathbf{q}) = \frac{1}{\|\mathbf{q}\|^2}\sum_{m=2L+1}^{4L}[\mathbf{J}]_{m,m}. \tag{60}$$

Unfortunately, (57) does not provide any clear indication about the impact of the system parameters on the ultimate accuracy achievable in the CFO estimation process. A more useful expression can be found by evaluating an approximate version of the CRB. The latter is obtained from the simplified model of the M vectors $\{\boldsymbol{\xi}_m; m = 0, 1, \ldots, M-1\}$ given in (28), combined with the white Gaussian noise assumption. Skipping the details for space limitations, the approximate CRB (ACRB) is found to be

$$\mathrm{ACRB}\{\phi\} = \frac{6\sigma_w^2}{MP^2(M^2-1)\left\|\mathbf{h}_{eq}\right\|^2} \tag{61}$$

and coincides with $\mathrm{var}(\hat{\phi}_{BLUE})$ given in (51).

VI. Simulation Results

A. Simulation Model

Computer simulations are conducted to examine the performance of the proposed methods in an OFDM WLAN system compliant with the IEEE 802.11a standard [1]. The DFT size is $N = 64$, while the sampling interval is set to $T_s = 50$ ns. This corresponds to a transmission bandwidth of 20 MHz with a subcarrier distance of 312.5 kHz. The synchronization schemes are applied to the STS placed in front of each frame. This sequence carries $N_p = 12$ non-zero pilot symbols, and is divided into $M_T = 10$ repeated parts, each containing $P = 16$ samples. After discarding the first two segments as the CP of the TP, the remaining $M = 8$ segments are exploited for CFO recovery. Hence, throughout simulations we let $P = 16$ and $M = 8$ unless otherwise specified. We adopt a discrete-time channel model and collect the samples of $v(t)$ into a vector $\mathbf{v} = [v(0), v(1), \ldots, v(L_v - 1)]^T$ of order L_v. The entries of $\mathbf{v}$ follow a circularly-symmetric Gaussian distribution with an exponentially decaying power delay profile

$$\mathrm{E}\{|v(k)|^2\} = \sigma_v^2\exp(-k/L_v) \quad k = 0, 1, \ldots, L_v - 1 \tag{62}$$

where $L_v = 4$ (with the only exception of Fig. 9) and σ_v^2 is chosen such that $\mathrm{E}\{\|\mathbf{v}\|^2\} = 1$. Both frequency independent and frequency selective RF imperfections are considered. If not otherwise stated, the LO-induced imbalance is characterized by $\alpha = 1$ dB and $\psi = 5$ degrees. The receive I/Q filters have discrete-time impulse responses $\mathbf{g}_I = [0, 1, \mu]^T$ and $\mathbf{g}_Q = [\mu, 1, 0]^T$ with $\mu = 0.1$, which results into overall CIRs $h[k]$ and $q[k]$ having support $k = 0, 1, \ldots, L-1$, with $L = L_v + 2$. These values have been previously adopted in the related literature [11] and represent a plausible model for I/Q mismatches. In addition to the aforementioned simulation set-up, in our study we also consider a more general scenario

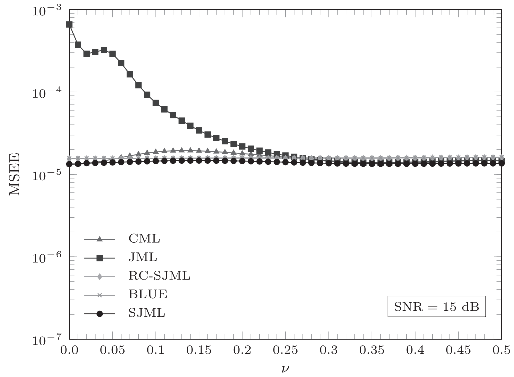

Fig. 2. Accuracy of the CFO estimators vs. ν with SNR = 15 dB.

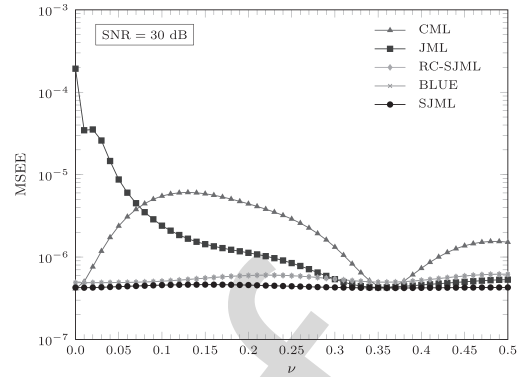

Fig. 3. Accuracy of the CFO estimators vs. ν with SNR = 30 dB.

wherein a coefficient $\rho \in [0, 4]$ is used to specify the values of the I/Q imbalance parameters as $\mu = 0.1\rho$, $\alpha = 1+0.122\rho$ and $\psi = 5\rho$ degrees. This allows us to assess the sensitivity of the considered schemes to the amount of RF imperfections, with $\rho = 0$ corresponding to an ideal situation where no I/Q imbalance is present.

Assuming a carrier frequency of 5 GHz and an oscillator instability of ± 30 parts-per-million (ppm), we obtain $|\phi|^{(\max)} = 0.015\pi$. This value falls well within the estimation range of the RC-SJML and BLUE, which is given by $|\phi| \leq \pi/P = 0.0625\pi$. When using SJML and RC-SJML, parameter N_ϕ is set to 128 since numerical simulations indicate that no significant improvement is achieved with $N_\phi > 128$.

B. Performance Assessment

The accuracy of the proposed frequency recovery schemes is assessed in terms of their mean square estimation error (MSEE). The estimated parameter is the CFO normalized by the subcarrier spacing, which is defined as $\nu = NT_s \Delta f$ or, equivalently, $\nu = N\phi/(2\pi)$. Recalling that $|\phi|^{(\max)} = 0.015\pi$, the uncertainty range of ν is given by $|\nu| \leq 0.48$. Comparisons are made with alternative ML-oriented methods, including the CML [24] and JML [11]. The complexity of these estimators has been evaluated in [23] and is reported in Table I. In writing these results we have borne in mind that the coarse search with CML can be efficiently performed through FFT techniques, while a similar approach cannot be adopted with JML.

Fig. 2 illustrates the MSEE of the CFO estimators as a function of ν measured at SNR=15 dB. We see that JML performs poorly for small CFO values, while the accuracy of the other schemes depends weakly on ν. The reason for the poor performance of JML when ν approaches zero is that this scheme aims at jointly estimating the channel distorted signal component $\mathbf{a} = \mathbf{\Gamma}_P(\phi)\mathbf{F}_P\mathbf{C}\mathbf{G}_2\mathbf{h}$ and its mirror image $\mathbf{b} = \mathbf{\Gamma}_P(-\phi)\mathbf{F}_P^*\mathbf{C}^*\mathbf{G}_2^*\mathbf{q}$ without effectively exploiting their mathematical model. Since in the absence of any CFO the mth received TP segment in (21) becomes $\mathbf{x}_m = \mathbf{a}+\mathbf{b}+\mathbf{w}_m$, there is no possibility for JML to get individual estimates of $\mathbf{a}$ and $\mathbf{b}$ in this specific situation. In contrast, the proposed algorithms can work satisfactorily for any CFO value as they exploit the inherent structure of $\mathbf{a}$ and $\mathbf{b}$, which makes these vectors resolvable even when $\nu = 0$. It is worth observing that CML, which is derived by ignoring the presence of I/Q imbalances, performs remarkably better than JML for $\nu < 0.15$. We also see that the accuracy of RC-SJML and BLUE is virtually the same as that of SJML, in spite of their reduced complexity.

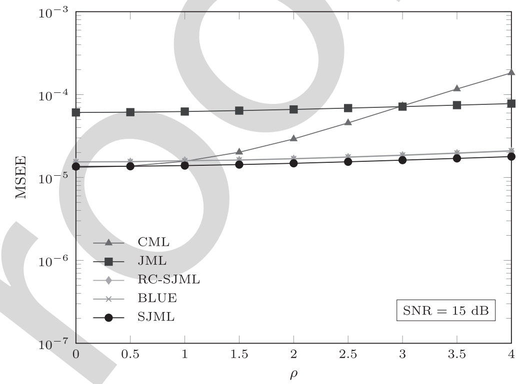

Fig. 4. Accuracy of the CFO estimators vs. ρ with SNR = 15 dB.

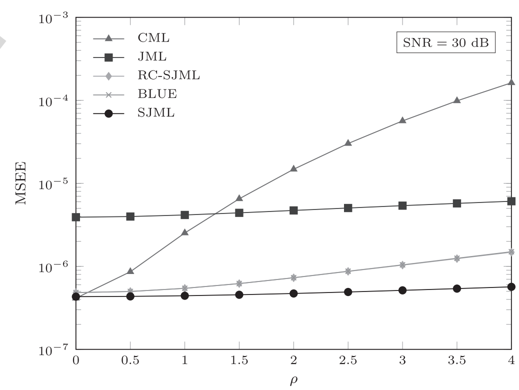

Fig. 5. Accuracy of the CFO estimators vs. ρ with SNR = 30 dB.

The results of Fig. 3 are obtained under the same operating conditions of Fig. 2, except that the SNR is now set to 30 dB. In such a case, the performance of CML exhibits large fluctuations as a function of ν, while the proposed schemes provide a remarkable accuracy irrespective of the CFO value. Again, JML performs poorly when ν approaches zero due to the impossibility of resolving vectors $\mathbf{a}$ and $\mathbf{b}$.

Figs. 4 and 5 show the MSEE of the CFO estimators as a function of ρ with ν uniformly distributed over the

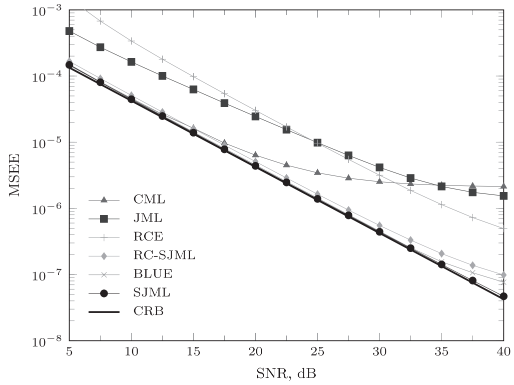

Fig. 6. Accuracy of the CFO estimators vs. SNR.

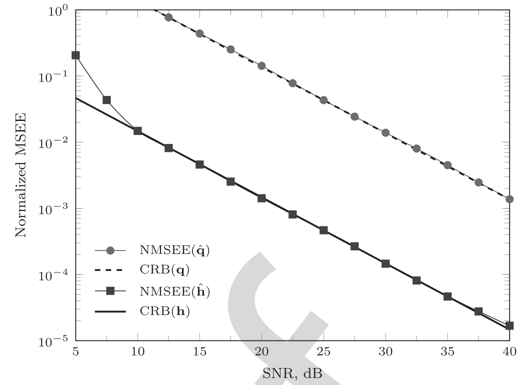

Fig. 7. Accuracy of the CIR estimates vs. SNR.

interval $[-0.5, 0.5]$. The SNR is 15 dB in Fig. 4 and 30 dB in Fig. 5. These results indicate that, irrespective of the SNR, the accuracy of JML and SJML is virtually independent of ρ, while CML is significantly affected by the amount of I/Q imbalances. As for RC-SJML and BLUE, they exhibit a remarkable resilience against RF imperfections at an SNR of 15 dB, while some performance degradation is observed at SNR = 30 dB in the presence of severe I/Q mismatches. However, these schemes largely outperform both JML and CML, while exhibiting a tolerable loss with respect to SJML.

Fig. 6 illustrates the accuracy of the investigated schemes as a function of the SNR when $\rho = 1$ and ν varies uniformly within the interval $[-0.5, 0.5]$. The curve labeled CRB corresponds to the bound reported in (57) and it is shown as a benchmark. Comparisons are also made with the reduced-complexity estimator (RCE) proposed in [25]. Although RCE was originally designed to operate with a TP composed of two identical halves, it can be applied to the 802.11a STS as well by considering such a sequence as the concatenation of two repeated segments $[\mathbf{x}_0^T\ \mathbf{x}_1^T \cdots \mathbf{x}_{M/2-1}^T]^T$ and $[\mathbf{x}_{M/2}^T\ \mathbf{x}_{M/2+1}^T \cdots \mathbf{x}_{M-1}^T]^T$. We see that SJML attains the CRB at any SNR value. Both RC-SJML and BLUE perform similarly to SJML (apart for a negligible loss in the high SNR region) and achieve a substantial gain with respect to JML and RCE. As for the CML curve, it keeps close to the CRB when SNR<15 dB, while it is plagued by a considerable floor at larger SNR values. Since our numerical analysis did not reveal any tangible difference between the true CRB and its approximation (61), we conclude that the noise term $w(t)$ in (2) can reasonably be modeled as a circularly symmetric white Gaussian process.

The accuracy of the estimated CIR vectors at different SNR values is assessed in Fig. 7 using the normalized MSEE (NMSEE) of $\hat{\mathbf{h}}$ and $\hat{\mathbf{q}}$, which is defined as

$$\mathrm{NMSEE}(\hat{\mathbf{h}}) = \frac{\mathrm{E}\left\{\left\|\hat{\mathbf{h}} - \mathbf{h}\right\|^2\right\}}{\mathrm{E}\{\|\mathbf{h}\|^2\}},$$

$$\mathrm{NMSEE}(\hat{\mathbf{q}}) = \frac{\mathrm{E}\left\{\left\|\hat{\mathbf{q}} - \mathbf{q}\right\|^2\right\}}{\mathrm{E}\{\|\mathbf{q}\|^2\}}. \tag{63}$$

Here, the estimate $\hat{\mathbf{u}} = [\hat{\mathbf{h}}^T\ \hat{\mathbf{q}}^T]^T$ is obtained as indicated in (17) letting $\tilde{\phi} = \hat{\phi}_{BLUE}$ and using the same operating scenario of Fig. 6. At medium and large SNR values, we see that both curves are tight to the relevant CRBs given in (59) and (60), while a certain discrepancy occurs in the low SNR region.

In order to assess the extent to which the approximation (22) can reasonably be adopted, it is interesting to investigate the impact of parameter P on the accuracy of the CFO estimate. For this purpose, in Fig. 8 we show the MSEE of the BLUE as a function of the SNR for $P = 16$, 32 and 64. Since the length of the TP is fixed to $MP = 128$, the corresponding values of M are 8, 4 and 2. In particular, the case $P = 32$ is handled by viewing the 802.11a STS as the concatenation of four repeated parts $[\mathbf{x}_0^T\ \mathbf{x}_1^T]^T$, $[\mathbf{x}_2^T\ \mathbf{x}_3^T]^T$, $[\mathbf{x}_4^T\ \mathbf{x}_5^T]^T$ and $[\mathbf{x}_6^T\ \mathbf{x}_7^T]^T$, with each vector $\mathbf{x}_i$ being composed of 16 elements, while the case $P = 64$ is tackled by dividing the TP into two parts $[\mathbf{x}_0^T\ \mathbf{x}_1^T\ \mathbf{x}_2^T\ \mathbf{x}_3^T]^T$ and $[\mathbf{x}_4^T\ \mathbf{x}_5^T\ \mathbf{x}_6^T\ \mathbf{x}_7^T]^T$. It turns out that, at SNR values smaller than 30 dB, the MSEE is practically the same with either $P = 16$ or 32, and keeps close to the relevant CRB given in (57). In contrast, very poor estimates are obtained with $P = 64$. It is worth noting that the formidable performance degradation incurred by the BLUE in passing from $P = 32$ to 64 cannot be totally ascribed to the approximation (22). Indeed, when $P = 64$ the estimation range of RC-SJML and BLUE is reduced to $|\phi| \leq 0.015625\pi$, which is only marginally greater than the value $|\phi|^{(\max)} = 0.015\pi$ adopted throughout simulations. In the presence of noise, we expect that the phase term $\theta(m)$ defined in (45) may occasionally experience jumps of 2π when $P\phi$ is close to $\pm\pi$ as a consequence of the wrapping phenomenon. Our analysis confirms the presence of these jumps when $P = 64$, which justifies the impressive loss of performance exhibited by the BLUE in this specific situation.

The results of Fig. 8 provide useful information about the maximum value of P that can be used with the BLUE. To see how this happens, we recall that the maximum phase error between $\mathbf{\Gamma}_P(\phi)$ and its approximation $e^{j(P-1)\phi/2}\mathbf{I}_P$ is $\Delta\phi^{(\max)} = (P-1)\,|\phi|^{(\max)}/2$. On the other hand, the MSEE curves in Fig. 8 indicate that, compared to the case $P = 16$, no penalty in estimation accuracy occurs when $P = 32$ and $|\phi|^{(\max)} = 0.015\pi$, yielding $\Delta\phi^{(\max)} \simeq \pi/4$. This means that a sufficient condition for applying the BLUE without incurring significant performance degradation

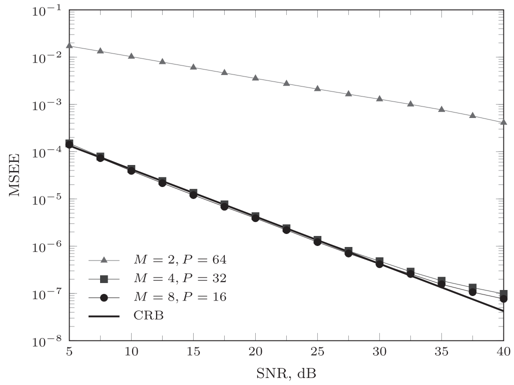

Fig. 8. Accuracy of the BLUE vs SNR for different values of P and $MP = 128$.

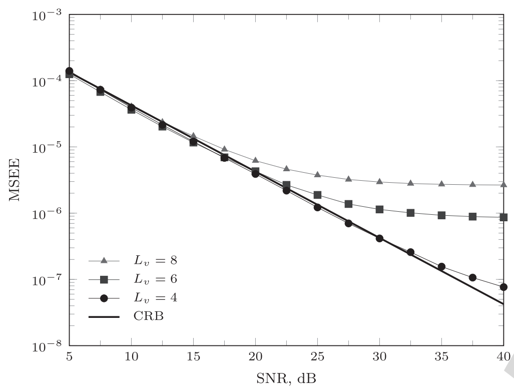

Fig. 9. Accuracy of the BLUE vs. SNR for different values of the channel order.

is $(P-1)\,|\phi|^{(\max)}/2 \le \pi/4$, which limits the range of P to

$$P \le 1 + \frac{\pi}{2|\phi|^{(\max)}}. \tag{64}$$

Fig. 9 illustrates the impact of the channel length on the performance of the BLUE when the constraint $L \le N_p/2$ is not fulfilled. In these simulations, the MSEE curves are obtained by designing the BLUE for a fictitious channel order $\overline{L_\upsilon} = 4$, (corresponding to $\overline{L} = \overline{L_\upsilon} + 2 = 6$), while the true values of L_υ are 4, 6 and 8. As expected, in the high SNR region the estimation accuracy exhibits an irreducible floor, which increases with the difference $L_\upsilon - \overline{L_\upsilon}$. On the other hand, all the curves attain the CRB when the SNR is smaller than 15 dB, thereby revealing an adequate resilience against a possible mismatch in the channel order.

We complete our analysis by comparing the investigated CFO recovery schemes in terms of their computational complexity. The last column of Tab. I shows the number of required flops when the algorithms are applied to a WLAN scenario with $P = 16$ and $M = 8$. Based on these results, we observe that SJML is hardly implementable due to its prohibitive complexity. A similar conclusion applies to JML which, in spite of its large computational load, provides poor performance when compared to BLUE and RC-SJML. Hence, leaving aside the SJML and JML, in Fig. 10 we report the number of flops required by the other explored schemes as a function of P. The curves are obtained by substituting

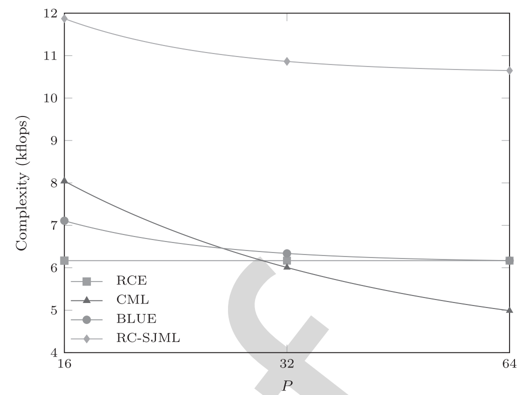

Fig. 10. Complexity of RC-SJML, BLUE, RCE and CML vs. P with $MP = 128$.

$MP = 128$, $L = 6$, and $N_\phi = 128$ in the expressions given in Tab. I. As is seen, the processing load of RCE is independent of P, while the complexity of the other algorithms decreases with P. These results indicate that the improved performance of RC-SJML with respect to existing alternatives (CML and RCE) is obtained at the price of an increase of the processing requirement by a factor of two. On the other hand, the BLUE attains the accuracy of RC-SJML with a computational load that is nearly the same as that of CML and RCE with either $P = 16$ or $P = 32$. Combining the MSEE measurements of Fig. 8 with the complexity analysis of Fig. 10, we conclude that $P = 32$ (and $M = 4$) is a good design choice when the BLUE is applied to a WLAN system compliant with the 802.11a standard.

VII. Conclusions

We analyzed the CFO estimation problem in an OFDM receiver plagued by frequency-selective I/Q imbalances. In doing so, we assumed that a repeated training preamble is available in front of each data packet to assist the synchronization task. Our first objective was the joint ML estimation of the CFO and channel impulse responses of the direct signal component and its mirror image. By exploiting knowledge of the pilot symbols embedded in the preamble, we derived a novel scheme (SJML) which eliminates the sign ambiguity problem of the JML estimator. Since implementation of SJML is impractical, we derived two alternative reduced-complexity schemes (RC-SJML and BLUE) by neglecting the phase rotation induced by the CFO within each TP segment. Upon considering a practical scenario compliant with the 802.11a WLAN standard, the following results were found: 1) both RC-SJML and BLUE lead to a drastic reduction of the processing load with respect to SJML without incurring any significant penalty in estimation accuracy; 2) compared to existing alternatives (CML, RCE, JML), RC-SJML exhibits a remarkable improvement of the system performance at the price of a certain increase of the computational load with respect to CML and RCE; 3) the BLUE attains the same performance of RC-SJML, while exhibiting a complexity similar to that of CML and RCE; 4) the length of the repetitive TP segment must be carefully designed in order to achieve a good trade-off between estimation accuracy, system complexity, and estimation range.

These conclusions indicate that the BLUE represents a practical solution for accurate CFO recovery in an OFDM direct-conversion receiver.

References

[1] *Wireless LAN Medium Access Control (MAC) and Physical Layer (PHY) Specifications, Higher Speed Physical Layer Extension in the 5 GHz Band*, IEEE Standard 802.11 WG, Sep. 1999.

[2] *IEEE Standard for Local and Metropolitan Area Networks, Part16: Air Interface for Fixed and Mobile Broadband Wireless Access Systems*, IEEE Standard 802.16, 2004.

[3] *Evolved Universal Terrestrial Radio Access (E-UTRA); Physical Channels and Modulation*, document 3GPP TS 36.211, 2012.

[4] W. Namgoong and T. H. Meng, "Direct-conversion RF receiver design," *IEEE Trans. Commun.*, vol. 49, no. 3, pp. 518–529, Mar. 2001.

[5] M. Valkama, M. Renfors, and V. Koivunen, "Advanced methods for I/Q imbalance compensation in communication receivers," *IEEE Trans. Signal Process.*, vol. 49, no. 10, pp. 2335–2344, Oct. 2001.

[6] F. Yan, W.-P. Zhu, and M. O. Ahmad, "Carrier frequency offset estimation for OFDM systems with I/Q imbalance," in *Proc. 47th IEEE Midwest Symp. Circuits Syst. (MWSCAS)*, vol. 2. Jul. 2004, pp. 633–636s.

[7] L. Lanante, Jr., M. M. Kurosaki, and H. Ochi, "Low complexity compensation of frequency dependent I/Q imbalance and carrier frequency offset for direct conversion receivers," in *Proc. IEEE Int. Symp. Circuits Syst. (ISCAS)*, Jun. 2010, pp. 2067–2070.

[8] S. D. Rore, E. Lopez-Estraviz, F. Horlin, and L. van der Perre, "Joint estimation of carrier frequency offset and IQ imbalance for 4G mobile wireless systems," in *Proc. Int. Conf. Commun. (ICC)*, vol. 5. Jun. 2006, pp. 2066–2071.

[9] Y.-C. Pan and S.-M. Phoong, "A new algorithm for carrier frequency offset estimation in the presence of I/Q imbalance," in *Proc. IEEE Veh. Techn. Conf. (VTC-Spring)*, Apr. 2010, pp. 1–5.

[10] M. Morelli and M. Moretti, "Carrier frequency offset estimation for OFDM direct-conversion receivers," *IEEE Trans. Wireless Commun.*, vol. 11, no. 7, pp. 2670–2679, Jul. 2012.

[11] G. Xing, M. Shen, and H. Liu, "Frequency offset and I/Q imbalance compensation for direct-conversion receivers," *IEEE Trans. Wireless Commun.*, vol. 4, no. 2, pp. 673–680, Mar. 2005.

[12] J. Park, Y. Lee, and H. Park, "Preamble design for joint estimation of CFO and I/Q imbalance for direct conversion OFDM system," *IET Commun.*, vol. 3, no. 4, pp. 597–602, 2009.

[13] C. J. Hsu, R. Cheng, and W. H. Sheen, "Joint least squares estimation of frequency, DC offset, I-Q imbalance, and channel in MIMO receivers," *IEEE Trans. Veh. Technol.*, vol. 58, no. 5, pp. 2201–2213, Jun. 2009.

[14] X. Cai, Y.-C. Wu, H. Lin, and K. Yamashita, "Estimation and compensation of CFO and I/Q imbalance in OFDM systems under timing ambiguity," *IEEE Trans. Vehic. Techn.*, vol. 60, no. 3, pp. 1200–1205, Mar. 2011.

[15] H. Lin, X. Zhu, and K. Yamashita, "Low-complexity pilot-aided compensation for carrier frequency offset and I/Q imbalance," *IEEE Trans. Commun*, vol. 58, no. 2, pp. 448–452, Feb. 2010.

[16] Y. C. Pan and S. M. Phoong, "A time-domain joint estimation algorithm for CFO and I/Q imbalance in wideband direct-conversion receivers," *IEEE Trans. Wireless Commun.*, vol. 11, no. 7, pp. 2353–2361, Jul. 2012.

[17] X. Wang, Y. Xue, L. Liu, F. Ye, and J. Ren, "Carrier frequency offset estimation in the presence of I/Q mismatch for wideband OFDM systems," in *Proc. IEEE 55th Int. Symp. Circuits Syst. (MWSCAS)*, Aug. 2012, pp. 924–927.

[18] R. Kume, H. Lin, and K. Yamashita, "Repeated preamble based carrier frequency offset estimation in the presence of I/Q imbalance," in *Proc. IEEE Int. Conf. Commun. (ICC)*, Jun. 2012, pp. 4867–4871.

[19] M. Morelli and H. Lin, "ESPRIT-based carrier frequency offset estimation for OFDM direct-conversion receivers," *IEEE Commun. Lett.*, vol. 17, no. 8, pp. 1513–1516, Aug. 2013.

[20] M. Morelli and M. Moretti, "A SAGE approach to frequency recovery in OFDM direct-conversion receivers," *IEEE Commun. Lett.*, vol. 18, no. 4, pp. 536–539, Apr. 2014.

[21] U. Tureli, H. Liu, and M. Zoltowski, "OFDM blind carrier offset estimation: ESPRIT," *IEEE Trans. Commun.*, vol. 48, no. 9, pp. 1459–1461, Sep. 2000.

[22] J. A. Fessler and A. O. Hero, "Space-alternating generalized expectation-maximization algorithm," *IEEE Trans. Signal Process.*, vol. 42, no. 10, pp. 2664–2677, Oct. 1994.

[23] A. A. D'Amico, L. Marchetti, M. Morelli, and M. Moretti, "Frequency estimation in OFDM direct-conversion receivers using a repeated preamble," *IEEE Trans. Commun*, vol. 64, no. 3, pp. 1246–1258, Mar. 2016.

[24] M. Ghogho, A. Swami, and P. Ciblat, "Training design for CFO estimation in OFDM over correlated multipath fading channels," in *Proc. Global Telecommun. Conf. (GLOBECOM)*, Nov. 2007, pp. 2821–2825.

[25] M. Asim, M. Ghogho, and D. McLernon, "OFDM receiver design in the presence of frequency selective I/Q imbalance and CFO," in *Proc. 21st Eur. Signal Process. Conf. (EUSIPCO)*, Marrakesh, Morocco, Sep. 2013, pp. 1–5.

[26] G.-T. Gil, I.-H. Sohn, J.-K. Park, and Y. H. Lee, "Joint ML estimation of carrier frequency, channel, I/Q mismatch, and DC offset in communication receivers," *IEEE Trans. Veh. Technol.*, vol. 54, no. 1, pp. 338–349, Jan. 2005.

[27] S. M. Kay, *Fundamentals of Statistical Signal Processing: Estimation Theory*. Englewood Cliffs, NJ, USA: Prentice-Hall, 1993.

[28] M. Morelli and U. Mengali, "An improved frequency offset estimator for OFDM applications," *IEEE Commun. Lett.*, vol. 3, no. 3, pp. 75–77, Mar. 1999.

Antonio A. D'Amico received the Dr.Ing. degree in electronic engineering and the Ph. D. degree from the University of Pisa, Italy, in 1992 and 1997, respectively. He is currently an Associate Professor with the Department of Information Engineering, University of Pisa. His research interests are in digital communication theory, with emphasis on synchronization algorithms, channel estimation, and detection techniques.

Michele Morelli received the Laurea degree *(cum laude)* in electrical engineering from the University of Pisa, Italy, in 1991, and the Ph.D. degree in electrical engineering from the University of Pisa. From 1992 to 1995, he was with the Department of Information Engineering, University of Pisa. In 1996, he joined the Centro Studi Metodi e Dispositivi per Radiotrasmissioni, Italian National Research Council, Pisa, where he was a Research Assistant. Since 2001, he has been with the Department of Information Engineering, University of Pisa, where he is a Professor of telecommunications. His research interests are in wireless communication theory, with emphasis on synchronization algorithms and channel estimation in multiple-access communication systems. He was a co-recipient of the VTC2006 (Fall) Best Student Paper Award. He has served as an Associate Editor for the IEEE TRANSACTIONS ON WIRELESS COMMUNICATIONS and the IEEE WIRELESS COMMUNICATION LETTERS. He is currently serving as an Associate Editor for the IEEE TRANSACTIONS ON COMMUNICATIONS.

Marco Moretti (M'03) received the degree in electronic engineering from the University of Florence, Florence, Italy, in 1995, and the Ph.D. degree from the Delft University of Technology, Delft, The Netherlands, in 2000. From 2000 to 2003, he was a Senior Researcher with Marconi Mobile. He is currently an Assistant Professor with the University of Pisa, Pisa, Italy. His research interests include resource allocation for multicarrier systems, synchronization, and channel estimation. He is an Associate Editor of the IEEE TRANSACTIONS ON SIGNAL PROCESSING.